Numerical Prediction of Submesoscale Flow in the Nocturnal Stable Boundary Layer over Complex Terrain

NELSON L. SEAMAN, BRIAN J. GAUDET, AND DAVID R. STAUFFER

Department of Meteorology, The Pennsylvania State University, University Park, Pennsylvania

LARRY MAHRT

College of Oceanic and Atmospheric Sciences, Oregon State University, Corvallis, Oregon

SCOTT J. RICHARDSON, JEFFREY R. ZIELONKA, AND JOHN C. WYNGAARD

Department of Meteorology, The Pennsylvania State University, University Park, Pennsylvania

(Manuscript received 17 February 2011, in final form 30 August 2011)

ABSTRACT

Numerical weather prediction models often perform poorly for weakly forced, highly variable winds in nocturnal stable boundary layers (SBLs). When used as input to air-quality and dispersion models, these wind errors can lead to large errors in subsequent plume forecasts. Finer grid resolution and improved model numerics and physics can help reduce these errors. The Advanced Research Weather Research and Forecasting model (ARW-WRF) has higher-order numerics that may improve predictions of finescale winds (scales $<\sim$20 km) in nocturnal SBLs. However, better understanding of the physics controlling SBL flow is needed to take optimal advantage of advanced modeling capabilities.

To facilitate ARW-WRF evaluations, a small network of instrumented towers was deployed in the ridge-and-valley topography of central Pennsylvania (PA). Time series of local observations and model forecasts on 1.333- and 0.444-km grids were filtered to isolate deterministic lower-frequency wind components. The time-filtered SBL winds have substantially reduced root-mean-square errors and biases, compared to raw data. Subkilometer horizontal and very fine vertical resolutions are found to be important for reducing model speed and direction errors. Nonturbulent fluctuations in unfiltered, very finescale winds, parts of which may be resolvable by ARW-WRF, are shown to generate horizontal meandering in stable weakly forced conditions. These submesoscale motions include gravity waves, primarily horizontal 2D motions, and other complex signatures. Vertical structure and low-level biases of SBL variables are shown to be sensitive to parameter settings defining minimum ''background'' mixing in very stable conditions in two representative turbulence schemes.

1. Introduction

It is well known that the rapid expansion of computer resources in recent decades has facilitated steady growth in numerical weather prediction (NWP) skill. However, while finer grid resolutions have been crucial for improving model accuracy, this alone has not always been sufficient. Better understanding and more accurate representation of atmospheric processes in the model physics have been needed to take full advantage of gains in resolution. For example, as model grid sizes of 2 $\sim$ 4 km have come into wider use, deep convection parameterizations have been eliminated so that all cloud and precipitation processes can be represented by explicit microphysics schemes. Generally, the combination of finer resolution and improved treatment of the moist physics has led to more accurate predictions of convective weather (e.g., Kain et al. 2006; Weiss et al. 2007). Besides issues related to model physics, a number of other factors can also limit the benefits of finer resolution: inaccurate numerics, poorly resolved surface heterogeneities and soil properties, insufficient observations, and inadequate data assimilation and initialization techniques

Corresponding author address: Nelson Seaman, Dept. of Meteorology, The Pennsylvania State University, University Park, PA 16802.
E-mail: seaman@ems.psu.edu

DOI: 10.1175/MWR-D-11-00061.1

(e.g., Weckwerth et al. 2004; Dabberdt et al. 2005; Ralph et al. 2005; Reen et al. 2006; Kang and Davis 2008). All of these contribute to reduce the predictability of atmospheric motions in high-resolution NWP models (Mass et al. 2002; Elmore et al. 2002; Stensrud and Weiss 2002; Rife et al. 2004; Rife and Davis 2005).

An especially difficult finescale forecast problem deals with predicting nonturbulent wind variability in the stable boundary layer and its impact on plume behavior. Efforts to reduce plume prediction errors by using high-resolution NWP models have often met with mixed results (Deng et al. 2004; Deng and Stauffer 2006). Besides the limitations of mesoscale models, our basic understanding of the SBL has also been limited by insufficient observations, instrument characteristics, and representativeness errors between time-averaged data at a point in space and gridcell quantities predicted by ensemble-averaged models (Gego et al. 2005; Mahrt et al. 2009).

Under clear skies and weak synoptic pressure gradients, radiative flux divergence typically leads to very stable nocturnal surface inversions that may have depths of only tens of meters or less, especially in the early evening (Smedman 1988; Mahrt and Vickers 2002; Vickers and Mahrt 2004; Mahrt et al. 2010). In the absence of strong dynamic forcing, horizontal thermal gradients form over sloping terrain, inducing gravity-driven currents (Sun et al. 2002). Quasi-steady drainage flow may ensue in relatively simple isolated environments, such as reported by Cuxart et al. (2007) over the island of Majorca, Spain, but many sites appear dominated by randomly fluctuating winds for which no steady state emerges (Mahrt 2009). The inherent predictability of motions in such cases can be rather poor.

In very stable nocturnal cases, turbulence can become extremely weak (Steeneveld et al. 2006; Wyngaard 2010). A typical 3D eddy length scale in the SBL may be only $\sim$1 m and turbulent kinetic energy (TKE) can be less than 0.1 $m^2\ s^{-2}$. Since buoyancy force dampens vertical motions in the stable regime, wind fluctuations can be mostly constrained to the horizontal direction (Mahrt 2007). Mahrt and Mills (2009) found that horizontal 2D fluctuations on the scale of 0.02 $\sim$ 2.0 km can easily dominate the mixing process in the SBL. Mestayer and Anquetin (1995) and Belusic and Mahrt (2008) define these small-scale nonturbulent motions as *submeso* to distinguish them from mostly turbulent *microscale* motions generally associated with unstable conditions. Although the physics remains poorly understood, Mahrt (2007, 2008) and Hiscox et al. (2010) demonstrated that when the speed of submeso and/or *mesogamma* (2–20 km) SBL motions is of the same order as the weakly forced mean synoptic speed, plume behavior generally exhibits large sudden directional shifts in addition to smoothly oscillating directional changes.

While Taylor's hypothesis assumes a direct correspondence between spatial and temporal scales of motion (Tennekes and Lumley 1972), it is a reliable approximation primarily for true turbulence. For convenience the present study will assume that a loose correspondence exists between the spatial (0.02–2.0 km) and temporal (<20 min) scales of nonturbulent submeso perturbations in a weakly forced stable flow (mean speed $< \sim$2.0 m s^{-1}). However, the precise temporal–spatial relationship in the submeso range remains unclear, given our current knowledge.

The strong stability and suppressed turbulence often found in weakly forced nocturnal cases favor poor dispersion conditions. These allow concentrations of SBL contaminants to persist for many hours, making them problematic for emergency planners. Therefore, our focus will be primarily in the zone below 10 m above ground level (AGL), as might be relevant for a toxic surface release into the atmosphere. Not only are the erratic direction changes caused by mesogamma and submeso motions poorly understood, they are unresolved in most current numerical predictions, thus presenting a very difficult forecast challenge. Model-predicted root-mean-square errors (RMSEs) for wind direction in the SBL can exceed 100°, even though the mean speed and vertical structure may be predicted quite well (Bravo et al. 2008). Thus, when studying boundary layer flow, Rife and Davis (2005) make a distinction between modeled structures having a simple qualitatively realistic physical structure and those having actual determinism (specific predictability). In short, even with advanced NWP models, it remains unclear which aspects of SBL flows might be predictable and under what circumstances.

Several mechanisms have been proposed for the erratic low-frequency submeso wind fluctuations, or *stable horizontal meandering*,[1] affecting near-surface plumes in weakly forced SBLs. Hanna (1983) suggested density-driven currents in complex terrain and gravity waves as the most probable causes. Multiple downslope currents evolving over even modestly uneven terrain may interfere with one another and with cold air pools forming at the lowest elevations, causing transient speed and direction variations at a given site (Mahrt et al. 2010). Internal gravity waves forced by imbalances between mass and velocity fields in a stable environment (Nappo 2002) are another likely source of nonstationarity. High in the free atmosphere, these gravity waves were found to be important contributors to the mesoscale kinetic

[1] In neutral or unstable boundary layers, meanders are often defined as changes in plume direction forced by 3D eddies larger than the plume width. However, the current discussion will be limited to the stable case.

energy spectra analyzed by Nastrom and Gage (1985) and were simulated in the Advanced Research Weather model (ARW) by Skamarock (2004). However, when they encounter the SBL, the behavior of these waves is less clear. Fritts et al. (2003) examined ducted gravity waves developing in elevated shear layers within deep SBLs over relatively flat terrain, and found that their influence damped rapidly toward the surface. Using idealized simulations, Poulos et al. (2000) demonstrated that the vertical propagation of mountain waves can interfere with and significantly alter near-surface SBL gravity currents. Cuxart and Jimenez (2007) used large-eddy simulation (LES) and tower observations to show that a dynamically unstable layer can form beneath the low-level jet (LLJ) atop the SBL, leading to periodic enhancements of jet shear, TKE generation, and fluctuating winds at the surface. Other possible mechanisms, such as vertical mixing events in the presence of directional shear and vortex shedding over complex terrain, have been suggested to explain the sudden large directional shifts encountered in the SBL (Etling 1990; Mahrt 1998, 2008; Anfossi et al. 2005). While a variety of mechanisms may be involved, NWP models (including their initial fields) generally have been inadequate to predict SBL wind fluctuations in a deterministic sense.

Historically, NWP models have been mostly ineffective for predicting even the most simple characteristics of realistic meandering behavior in nocturnal SBLs because (i) model resolution has usually been too coarse to resolve the mesogamma-scale terrain irregularities and internal gravity waves largely responsible for wind fluctuations in the SBL, (ii) model turbulence physics may be inadequate in highly stable conditions near the surface, and (iii) observations are often insufficient to initialize and verify mesogamma and submeso scales of motion. Given the limitations of most NWP models, atmospheric transport and dispersion (AT&D) prediction models have been forced either to ignore or crudely parameterize the effects of nonturbulent mesogamma and submeso scales of motion that can easily dominate the SBL mixing process. For example, Sykes et al. (1993, 1998) include a diffusion-like term in their Lagrangian puff model to account statistically for unresolved mesogamma and submeso fluctuations. As a result, predicted plumes in stable meandering flow often appear overly diffuse and may underestimate embedded maximum concentrations.

The purpose of this paper is to explore the predictability of wind and temperature fluctuations associated with mesogamma and submeso stable meandering in the nocturnal SBL on time scales from minutes to hours. For this purpose, we will use subkilometer horizontal grid spacing in an NWP model configured for very stable nocturnal conditions. To facilitate meaningful model evaluations, we will make use of a practical method for defining and isolating predictable components in time series data versus the more rapidly fluctuating nondeterministic components (Gaudet et al. 2008). Section 2 will describe the NWP model and the design of the numerical experiments. Section 3 will describe a local field network used to provide special data for SBL analysis and model verification. Section 4 will report model evaluation results, while section 5 will briefly summarize the investigation.

2. Numerical model and experiment design

a. The Advanced Research WRF model

The NWP model chosen for this research is the Weather Research and Forecasting model (WRF) system known as ARW-WRF version 2.2 (Skamarock et al. 2007). ARW-WRF is designed with a terrain-following sigma-pressure vertical coordinate and options for higher-order spatial differencing on the Arakawa-C grid. Here, the ARW-WRF's fifth-order horizontal finite-differencing advection scheme was selected, along with a third-order scheme for vertical advection and the third-order Runge-Kutta scheme for time integration. These odd-order schemes are designed to maximize the accuracy of small-scale waves (Wicker and Skamarock 2002). However, they can also introduce an indeterminate amount of implicit diffusion (generally considered small). Based on comparisons of observed and predicted kinetic energy spectra in the free atmosphere, Skamarock (2004) estimated the model's effective resolution to be roughly $7\Delta x$, where Δx is the horizontal mesh size.

b. Baseline model configuration

To study local SBL flow, ARW-WRF was configured with four nested-grid domains having one-way nest interfaces. The outermost 12-km domain covers the entire contiguous United States (CONUS), with a second 4-km domain defined over the mid-Atlantic region (Fig. 1). Smaller 1.333- and 0.444-km domains are embedded over central Pennsylvania (PA). The finest domain has 151×151 horizontal points (Table 1) centered on the Nittany Valley and its surroundings (Fig. 2). The terrain of central PA is dominated by the Allegheny Mountains ($\sim$700 m MSL, 15–20-km width) in the northwest part of the finest domain, while the rest of the domain contains narrow quasi-parallel ridges reaching $\sim$600 m MSL and having widths of $4 \sim 5$ km. These ridges flank broader valleys oriented roughly southwest–northeast. Because the ridges extend 300–350 m above the valley floors, they strongly influence near-surface winds, especially in stable conditions. The narrow width of the ridges makes subkilometer grids important to resolve local circulations.

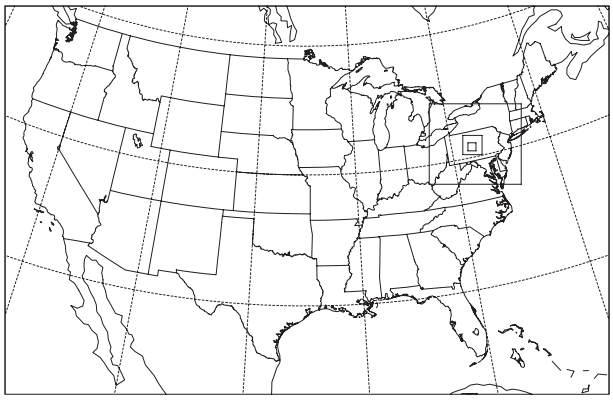

FIG. 1. ARW-WRF four-domain nested-grid configuration.

In the absence of strong dynamical forcing, surface radiative and turbulent fluxes are the dominant forcing of the nocturnal SBL structure (Ha and Mahrt 2003; Steeneveld et al. 2006). Vickers and Mahrt (2004) showed that the weakly turbulent, undisturbed nocturnal SBL over land in early evening can often be described as the layer where the buoyancy flux (BF) decreases more or less linearly from a maximum negative surface value to nearly zero at its top. This very stable nocturnal boundary layer frequently has a depth of $h \sim 20$–50 m, roughly the thickness of the lowest one or two layers in most general-use mesoscale NWP models today, although because of clear-air radiative cooling, the atmosphere may be modestly stable through a considerably deeper layer (Andre and Mahrt 1982). Thus, to investigate the structure and evolution of nocturnal SBL processes, the model's vertical grid must be considerably finer than normal (e.g., Soderberg and Parmhed 2006; Steeneveld et al. 2006; Cuxart et al. 2006). Here, the baseline model configuration has 43 layers in all four domains with the lowest 5 layers each having a 2-m thickness, with gradually increasing thicknesses thereafter up to the model top at 50 hPa. This provides 11 layers in the lowest 68 m AGL (Fig. 3a).

Even for the innermost domain, turbulent eddies in the nocturnal SBL are much smaller than the grid ($\Delta x = 0.444$ km) so a mesoscale model with parameterized ensemble-mean turbulence remains sufficient (Wyngaard 2010). However, with such a fine grid, this type of turbulence scheme is not recommended for unstable boundary layers exceeding a 1-km depth, because Δx then approaches the scale of the energy-containing turbulence, l, and ensemble-mean formulations cannot resolve turbulence, by definition. Instead, a large-eddy simulation with equations of motion filtered according to $l \gg \Delta x$ and equipped with a Smagorinsky (1963) eddy-viscosity closure or similar subgrid-scale filter would be more appropriate.

TABLE 1. Resolution and size of the four nested-grid ARW-WRF domains.

Domain No.	Horizontal grid increment (km)	Time step (s)	Horizontal grid dimensions
1	12.000	30	421 × 271
2	4.000	15	193 × 169
3	1.333	5	121 × 121
4	0.444	2	151 × 151

Most experiments in this study use the standard version of the 1.5-order Mellor–Yamada–Janjic (MYJ) turbulence scheme (Janjic 2002) available in the WRF system. This scheme has a prognostic equation for TKE, is designed for all stability classes, and has undergone extensive evaluation in research and operational applications. Additional model physics include a two-stream broadband radiation scheme and simple microphysics for cloud water–ice and rain–snow (Dudhia 1989). Surface fluxes are calculated using a simple five-layer thermal diffusion land surface scheme (Grell et al. 1994). The 1.333- and 0.444-km domains that are of greatest interest here are dominated by deciduous forests and crop–pasture lands. These land types have a surface momentum roughness length of $z_0 = 0.50$ and 0.15 m, respectively, and a much smaller thermal roughness (a function of momentum roughness and the scale velocity, u^*), especially when the bulk Richardson number exceeds 0.2.

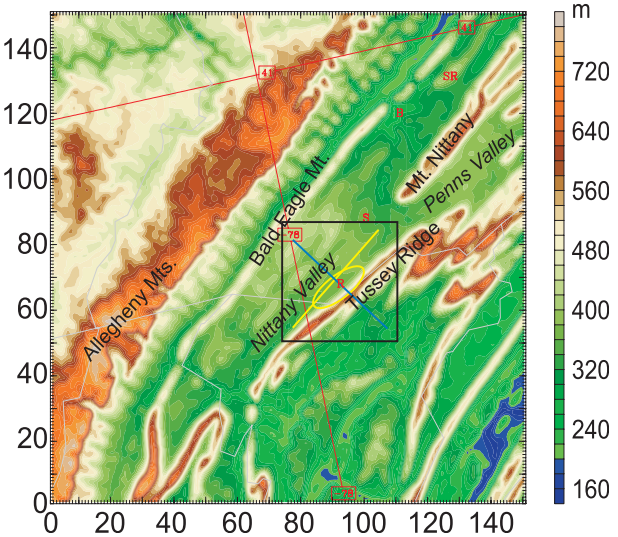

FIG. 2. Topography on the innermost ARW-WRF domain, horizontal resolution $\Delta x = 444$ m. Yellow ellipse marks area of local observing network. Black square denotes location of subdomain for display of detailed features. Yellow and blue line segments inside the black square indicate locations of vertical cross sections.

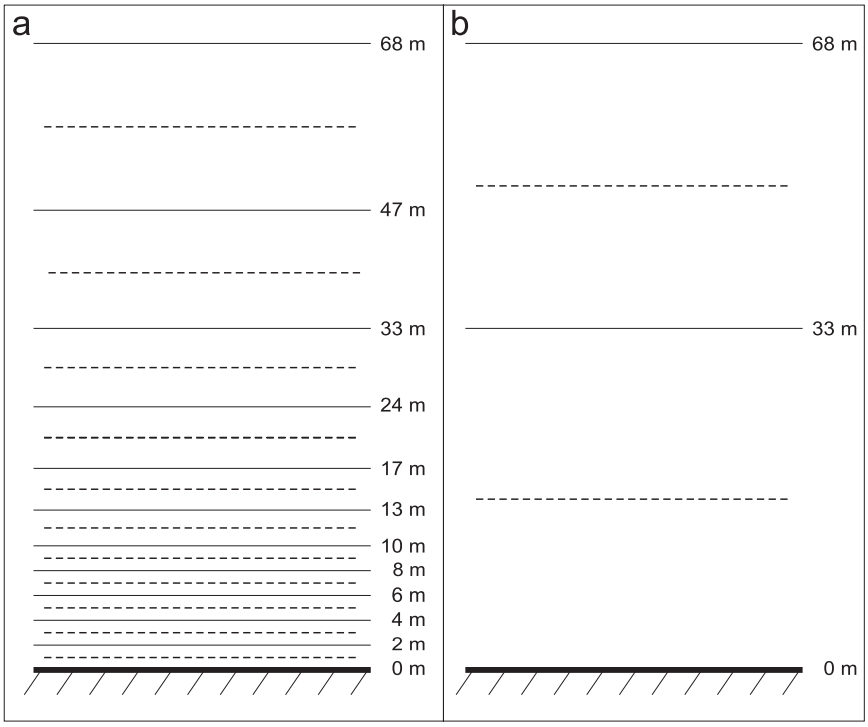

FIG. 3. ARW-WRF vertical layer configurations below 68 m AGL: (a) baseline configuration and (b) conventional vertical-resolution configuration.

Plant canopy effects are ignored in this study. Parameterized deep convection (Kain and Fritsch 1993, 1998) is invoked only in the 12-km domain.

Beginning in September 2007, forecasts using the baseline configuration (Experiment Baseline in Table 2) were run daily for the 12-h nocturnal period beginning at 0000 UTC (1900 LST in PA). To satisfy stability criteria on the fine vertical grid, time steps on the 0.444-km domain are $\Delta t = 2$ s (Table 1). Initial conditions and lateral boundary conditions are interpolated from the National Centers for Environmental Prediction (NCEP) 0.5° Global Forecast System (GFS) analyses using the WRF Preprocessing System (WPS). Complete ARW-WRF output files for the 1.333- and 0.444-km domains are saved at 12-min intervals, while files for the outer two domains are saved every hour. Also, 3D output files are saved at 10-s intervals over a subdomain area covering a special field measurement network in Nittany Valley (28×28 grid cells of the 0.444-km domain and 10×10 cells of the 1.33-km domain; also see section 3) and at all levels up to 500 hPa to support detailed analyses of high-frequency fluctuations.

c. Sensitivity experiment design

To better understand the influence of model resolution on submeso motions predicted in the shallow nocturnal SBL, three experiments were designed with horizontal and/or vertical grids more typical of conventional mesoscale model configurations (Table 2). Experiment LrgDX uses $\Delta x = 1.333$ km while retaining the very fine 43-layer vertical resolution of Experiment Baseline (Fig. 3a). In Experiment LrgDZ, the highest-resolution, 0.444-km grid is retained, but the lowest 11 vertical layers of Experiment Baseline are fused into 2 layers, so that the lowest layer becomes ~33 m deep (Fig. 3b). Thus, the total number of layers in Experiment LrgDZ is reduced to 34, while above 68 m AGL all layers are identical to Experiment Baseline. Finally, Experiment LrgDXDZ combines the coarser horizontal grid of $\Delta x = 1.333$ km and 34-layer vertical grid.

Last, two additional sensitivity experiments were designed to examine the influence of alternative turbulence physics on predicted SBL structure and near-surface submeso motions. Most turbulence schemes contain limiting parameters that impose a minimum amount of mixing to maintain numerical stability in very stable conditions (Brost and Wyngaard 1978). However, given sufficient stability, buoyancy forces in the atmosphere may remove energy from the energy-containing turbulent eddies faster than it can be generated by wind shear, effectively extinguishing the rest of the turbulence (Wyngaard 2010). Analysis has suggested that the minimum background default values for turbulent kinetic energy $\mathrm{TKE}_{\mathrm{MIN}}$ and length scale l_B in the standard MYJ scheme (Table 2) may

TABLE 2. Design for the Baseline Expt and five sensitivity experiments.

Expt name	Finest horizontal grid (km)	Lowest layer depth (m)	Total vertical layers	No. of layers below 68 m AGL	TKE_{MIN} (m^2 s^{-2})	l_B (m)
Baseline	0.444	2	43	11	0.10	0.32
LrgDZ	0.444	33	34	2	0.10	0.32
LrgDX	1.333	2	43	11	0.10	0.32
LrgDXDZ	1.333	33	34	2	0.10	0.32
ModMYJ	0.444	2	43	11	0.01	0.10
QNSE	0.444	2	43	11	0.01	0.32

impose too much residual mixing in very stable nocturnal SBLs (Z. Janjic 2008, personal communication). Table 2 shows that the values of these parameters were reduced in Experiment ModMYJ compared to the standard MYJ scheme.

A second alternative turbulence parameterization by Sukoriansky et al. (2006), called Quasi-Normal Scale Elimination (QNSE), has recently been installed in ARW-WRF. This fairly new scheme derives spectral expressions for eddy viscosity and eddy diffusivity based on quasi-Gaussian mapping of the velocity and temperature fields. The model implies scale-dependent partial averaging of both turbulence and internal waves as one entity, and is designed to perform well in weakly mixed very stable conditions. As invoked in the WRF model and tested in Experiment QNSE, the QNSE turbulence scheme also defines parameters for minimum mixing conditions, similar to the MYJ scheme (see Table 2).

3. Local observing network

As explained in section 2, very fine horizontal and vertical grid resolutions are necessary to resolve the complex terrain and interactive physical processes likely to dominate submeso motions in shallow nocturnal SBLs in central PA. However, the temporal and spatial scales resolved by the standard synoptic observing network are much too coarse to allow meaningful evaluation at the submeso scales. Therefore, a special network of instrumented towers was deployed in a portion of Nittany Valley to provide continuous high-frequency wind and temperature measurements for evaluation of the subkilometer ARW-WRF model predictions.

When designing a measurement network, site distribution, instrument type, and sampling rates are established based on the spatial and temporal scales of features to be monitored (Belusic and Mahrt 2008). In this case instruments were deployed at intervals ranging from 100 ~ 200 m up to 3 km to support investigations of submeso and mesogamma scale features in stable conditions. Wind and temperature measurements in the lowest few meters AGL are important for observing very shallow gravity-induced downslope winds. Since submeso SBL flows become important mainly with very weak winds and include frequent sudden changes of wind direction, high-accuracy fast-response wind sensors are required. Ideally, measurements up to 30 ~ 50 m AGL are useful for studying SBL depths. Relatively few existing or historical measurement networks meet all these criteria.

For the current study a small prototype network of six short instrumented 2- and 10-m towers and a taller 50-m tower was deployed in late summer 2007 over gently rolling terrain at Rock Springs in Nittany Valley, just northwest of Tussey Ridge (Fig. 2, yellow ellipse). The primary wind instrumentation consisted of Vaisala WS-425 2D 1-Hz sonic anemometers at 2, 3, and 10 m AGL. These anemometers have a very low startup threshold (manufacturer's specifications say "virtually zero"), 1-Hz sampling rate, and ~0.10 m s^{-1} accuracy. In addition, 10 Campbell Thermistors were mounted at 2 and 9 m AGL. The towers were deployed in two intersecting lines approximating a "T" (Fig. 4). One ~3-km line was oriented along the valley floor roughly parallel to Tussey Ridge, while the other line was ~1 km in length oriented roughly perpendicular to the ridge. In autumn 2008, the 50-m tower at site 10 was equipped with a 2D sonic instrument at 17 m and Vaisala 3D 20-Hz sonic anemometers at 34 and 47 m AGL. All instruments have very low power requirements and no moving parts, which minimizes maintenance requirements. Each tower is outfitted with a battery-powered solar rechargeable data recorder to provide continuous operations and a radio transmitter to relay the data to a central network computer. Once at the central computer, the raw 1- and 20-Hz data are quality checked, reformatted into 1-min averages, distributed to users, and archived.

4. Model evaluations

Most of the model evaluations in central PA reported here are limited to nocturnal cases with synoptic conditions favoring the development of very stable SBLs. Case selection criteria, based solely on aviation routine

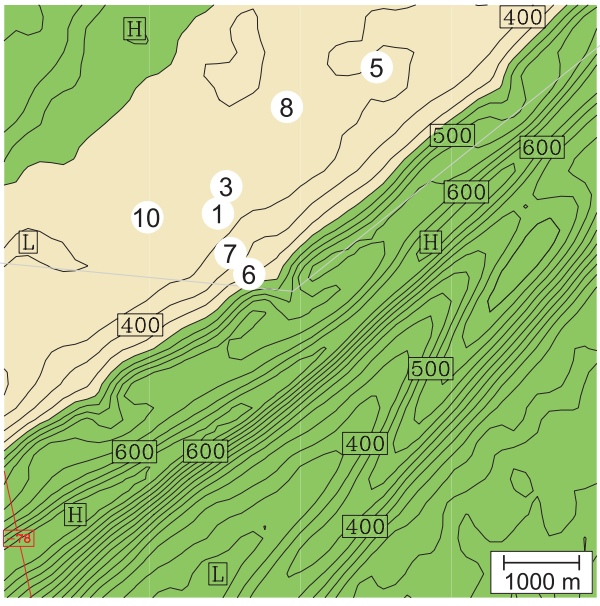

FIG. 4. Detail of the vicinity around Rock Springs showing location of instrumented towers in Nittany Valley. Tussey Ridge is to the south. Green shading indicates mostly deciduous hardwood forest. Lighter tan shading represents agricultural land. Contours are terrain height (m).

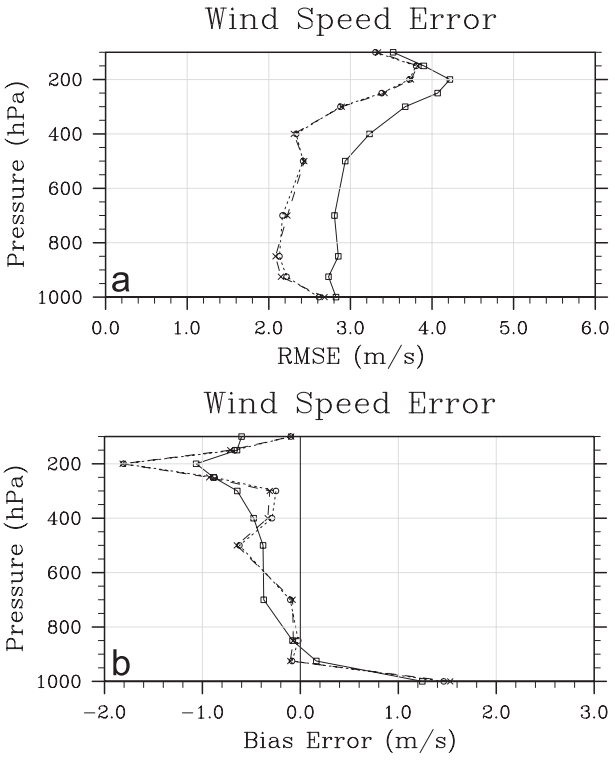

FIG. 5. Domain-averaged wind speed errors [(a) RMSE and (b) bias error; m s^{-1}] at 1200 UTC on full ARW-WRF 12-km domain (solid) and 4-km domain (dashed) in Expt Baseline as a function of pressure (hPa). Dotted line shows error calculated from 12-km ARW-WRF solution, but only over area of the 4-km domain.

weather report (METAR) data at State College, PA (SCE), require no more than 2 h of cloud cover between 0000 and 1200 UTC and no precipitation. These criteria are only moderately restrictive to allow a variety of mostly clear stable cases to be considered. Site- and case-specific evaluations on the 1.333- and 0.444-km domains focus on three periods: mid-autumn 2007, late spring 2008, and September 2009. Conventional domainwide statistical evaluations also are performed on the 12- and 4-km domains for the periods in 2007 and 2008.

a. Coarse domains

Since the high-resolution 1.333- and 0.444-km domains cover such a small area in central PA, model errors originating on the two outer domains can propagate through the nest interfaces and potentially dominate local SBL solutions. Thus, we begin with a brief evaluation of RMSEs and bias errors on the coarse 12- and 4-km domains.[2] Figures 5–7 present model error profiles in Experiment Baseline versus 1200 UTC (0700 LST in PA) radiosonde data for wind speed, wind direction, and temperature, respectively. The profiles summarize domain-averaged statistics based on 31 cases meeting the diagnostic criteria for probable SBL development in PA composited for two periods: 19 cases in October–November 2007 and 12 cases in June 2008.

The RMSEs of model-predicted wind speed (Fig. 5a) display a typical pattern, with the smallest errors in the lower troposphere (2–3 m s^{-1}) and maximum errors near the tropopause (3.5 ~ 4.5 m s^{-1}). Bias scores (Fig. 5b) indicate that model speeds are 1.0 ~ 1.5 m s^{-1} too fast at 1000 hPa on both domains, but then develop a slightly negative bias (<1 m s^{-1}) through the rest of the troposphere. RMSEs are 0.5 ~ 1.0 m s^{-1} greater on the large 12-km domain, but overall the profiles for the two domains exhibit mostly similar trends and magnitudes. When 12-km errors are recalculated only over the area of the 4-km domain, they closely match those of the 4-km model solution. This indicates that the greater RMSEs on the full 12-km domain are probably due to inclusion of the Rocky Mountains. Apparently, the 4-km grid resolution adds little to the 12-h forecast accuracy through most of the column, at least over this region. The errors shown here are mostly similar to those simulated with ARW-WRF on a 5-km CONUS domain

[2] Domainwide statistics were calculated using the Model Evaluation Toolkit (MET), a supported set of standardized community codes provided by the WRF Developmental Testbed Center (DTC) in Boulder, Colorado (Holland et al. 2007).

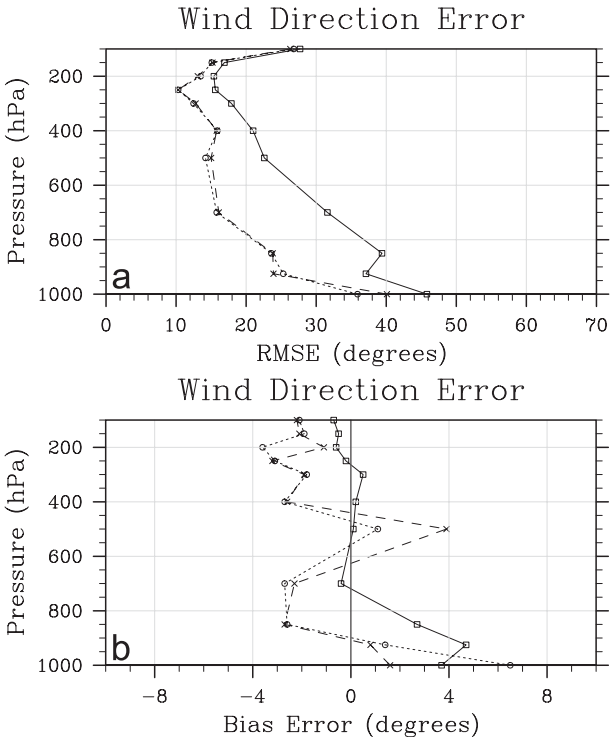

FIG. 6. As in Fig. 5, but for wind direction errors (°).

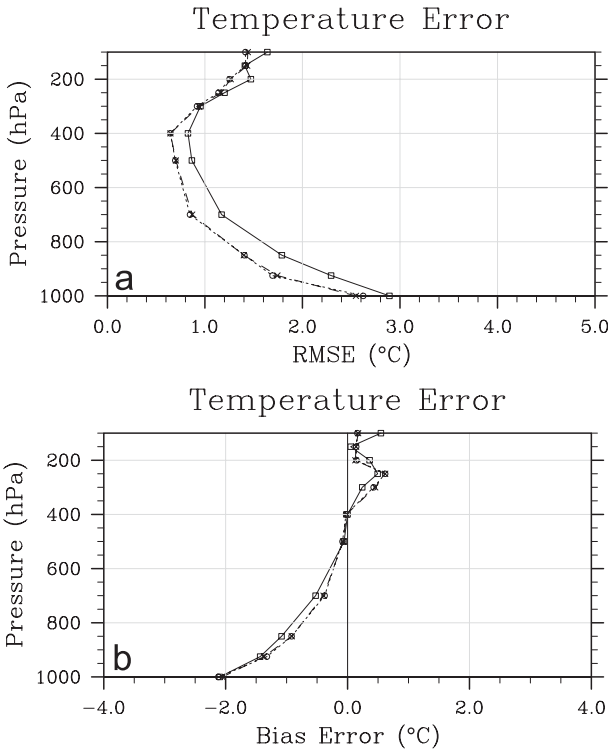

FIG. 7. As in Fig. 5, but for temperature errors (°C).

by Koch and Gall (2005) in 74 wintertime cases (not shown). However, they found significantly larger RMSEs, perhaps due to the stronger mean baroclinicity in winter compared to the mid-autumn and late spring seasons.

Next, Fig. 6a reveals large RMSEs of 35° ~ 45° for the wind direction at 1000 hPa on both domains. This result is quite common for near-surface model forecasts with similar Δx, likely because of unresolved surface heterogeneities (e.g., Schroeder et al. 2006), but as expected the errors rapidly decrease with height. Note that the RMSEs are 10° ~ 20° smaller on the 4-km domain than on the larger 12-km domain at most levels. While some of this improvement might be attributed to the finer horizontal grid resolution, a comparison to the 12-km solutions only over the same area as the 4-km domain shows it is again likely that the absence of the Rocky Mountains in the 4-km domain contributes significantly to the greater apparent skill of the smaller domain. Meanwhile, Fig. 6b shows that biases in wind direction remain small and nearly random, less than ~4°, throughout the column. This confirms that the overall accuracy of model-predicted winds is quite reasonable on both outer domains.

Figure 7 indicates that 1200 UTC temperature errors near 1000 hPa are somewhat large on both domains, with low-level cool biases of ~−2°C and RMSEs of 2.5° ~ 3.0°C. Above 850 hPa, temperature errors drop dramatically and then slowly rise again near the tropopause, where there is a slight warm bias of ~0.5°C and RMSEs grow to 1.4° ~ 1.6°C. The domainwide cold biases at 1000 hPa may be due in part to the simple five-layer soil submodel used in this study, which specifies soil moisture only as a function of land use and season, without considering antecedent rainfall. The simple soil scheme was selected for this initial investigation to minimize the complexity of feedbacks allowed between the surface and atmosphere, making for easier interpretation of local physics in the SBL. This scheme will be replaced in the future by the WRF's more detailed Noah land surface model (Chen and Dudhia 2001a,b).

Complementing the vertical error profiles, similar error statistics for 10-m winds and 2-m temperatures were calculated every 3 h for 91 spring and autumn cases on the two coarse-grid domains for Experiment Baseline (Table 3).[3] As expected, surface errors are mostly similar to those reported at 925 and 1000 hPa in Figs. 5–7, but tend to reflect somewhat enhanced influences due to local surface heterogeneities. The table shows fairly consistent positive speed biases of 1–1.5 m s^{-1} in the ARW-WRF 10-m winds through the forecast period. The

[3] Surface statistics were based on all cases in the October–November and June periods, not only the cases favoring SBL development in central PA.

TABLE 3. Domain-averaged surface errors vs forecast hour for 91 cases of Expt Baseline in October–November 2007 and June 2008.

Variable	Error score	Domain (km)	Forecast hour 0	3	6	9	12
10-m speed (m s^{-1})	RMSE	12	2.1	2.3	2.4	2.4	2.3
		4	2.0	2.0	2.0	2.0	1.9
	Bias	12	0.0	1.2	1.4	1.4	1.1
		4	0.6	1.1	1.3	1.3	0.9
10-m direction (°)	RMSE	12	44.3	45.2	47.1	47.7	48.4
		4	45.4	46.8	46.0	48.9	47.3
	Bias	12	2.9	1.6	5.5	5.6	4.3
		4	3.4	0.5	2.0	2.8	0.7
2-m temperature (°C)	RMSE	12	3.9	3.5	3.4	3.4	3.8
		4	4.1	3.5	3.6	3.5	4.1
	Bias	12	−2.9	−2.2	−1.5	−1.2	−1.6
		4	−3.2	−2.4	−1.9	−1.4	−2.2

RMSEs for speed on both the 12- and 4-km domains remain almost unchanged from their initial values through the entire nocturnal period. Also similar to the upper-level statistics, the spring–autumn 10-m wind speed RMSEs in the 12-km CONUS domain of Experiment Baseline are ~25% smaller than wintertime RMSEs found by Koch and Gall (2005) in the first 12 h of their 5-km ARW-WRF forecasts.

Table 3 also shows statistics for the evolution of surface wind direction errors through the 12-h nocturnal forecasts for the autumn and spring seasons. First, it is clear that RMSEs for direction are quite large in the model's initial conditions, but they grow very little over time, even though cases with very weak observed speeds (<1.0 m s^{-1}) are excluded from these calculations. Surface direction biases are initially small but tend to become more positive (clockwise errors) during the night on the 12-km domain, which, along with the positive surface speed bias, is consistent with possibly excessive background turbulent mixing of momentum in the SBL.

Finally, the table presents ARW-WRF forecast errors for 2-m surface temperatures. The RMSEs appear rather large, but are already in the initial conditions at 0000 UTC (3°–4°C). Many of the RMSEs may be explained by initial cold biases of ~−3°C, which are partly moderated during the course of the forecasts [from ~(−1.6° to 2.2°C) by 1200 UTC]. Although initial condition errors from the GFS analyses certainly affect the forecasts, the ARW-WRF surface errors may also be related to the relatively simple five-layer land surface model used in the study. Again, there do not appear to be any clear systematic differences in the errors between the 12- and 4-km domains. In summary, surface statistics on the two coarse domains indicate that the ARW-WRF high-resolution baseline configuration with the standard MYJ turbulence scheme produces generally skillful predictions of the state variables in stable nocturnal conditions, despite a tendency for some positive biases in surface winds and cool biases in temperatures. Given the modest size of these biases, model solutions on the inner 1.333- and 0.444-km domains should not be overly affected by synoptic-scale errors in most cases.

b. Fine domain simulations at Rock Springs

In weakly forced, mostly clear nocturnal cases over central PA, surface radiation flux divergence and turbulence flux usually dominate the development of the SBL, producing a strong thermal inversion in the lowest few tens of meters AGL. Lapse rates in these layers often exceed 0.1°C m^{-1} and TKE may become less than ~0.1 m^2 s^{-2}. Above this intense nocturnal SBL, a deeper but somewhat less stable quiescent layer may extend upward a few hundred meters (e.g., Mahrt et al. 1998; Steeneveld et al. 2006). Sufficient wind shear may develop occasionally near the top of this deep stable layer to generate moderate turbulence aloft (0.1 ~ 1.0 m^2 s^{-2}), independent of the surface drag (Smedman 1988; Banta et al. 2007). However, unless the two turbulent layers become connected, most often because of intermittent downward transport of TKE (Mahrt and Vickers 2002), it is the shallow, intensely stable layer close to the ground that will define the SBL here.

Numerous methods have been proposed for defining the SBL depth h. Diagnostics for an equilibrium SBL depth h_E generally fall into two categories: surface flux–based methods (e.g., Zilitinkevich et al. 2007; Steeneveld et al. 2007) and Richardson number–based methods (e.g., Vogelezang and Holtslag 1996). In practice these fairly idealized equilibrium methods often encounter difficulty because of nonsteady effects: large-scale baroclinicity,

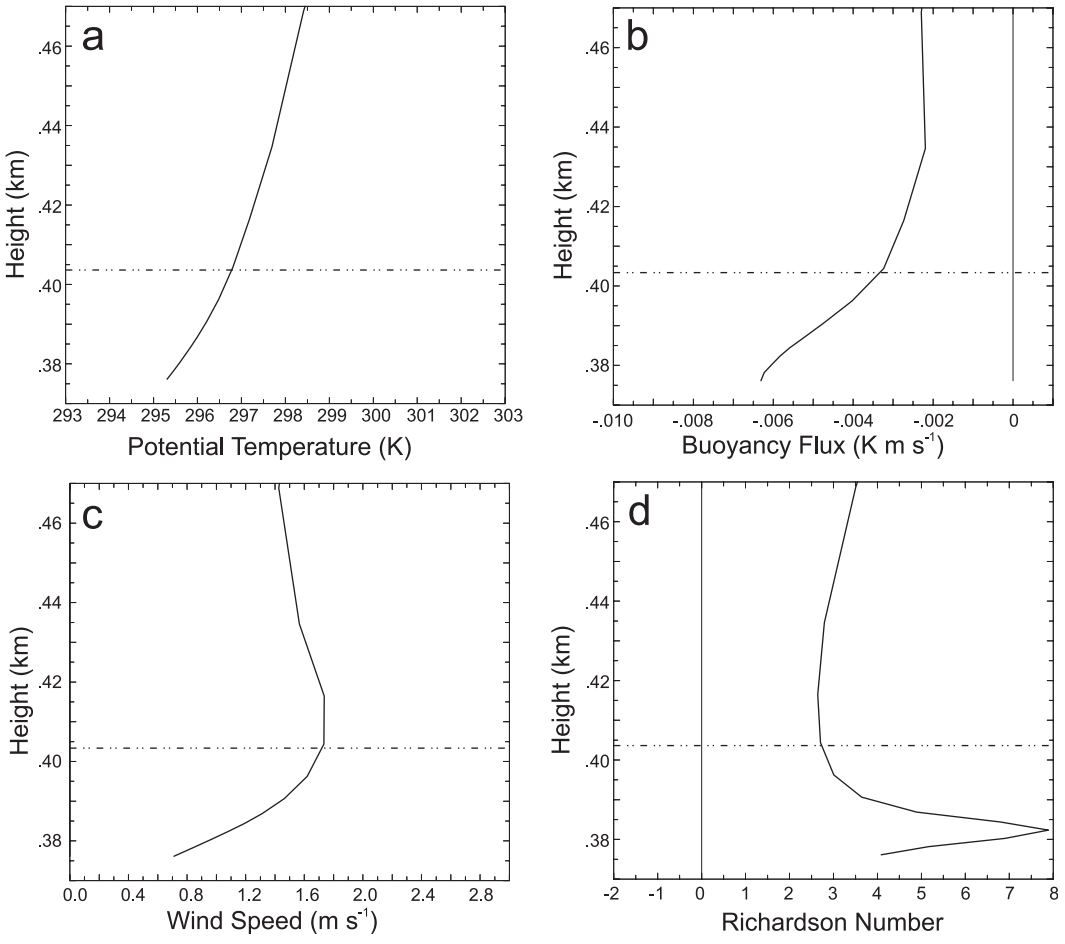

FIG. 8. Vertical profiles predicted in the lowest 100 m AGL of Expt Baseline for (a) potential temperature (K), (b) buoyancy flux (K m s^{-1}), (c) wind speed (m s^{-1}), and (d) Richardson number at site 3, elevation 375 m MSL, on the 0.444-km domain at Rock Springs at 0200 UTC 10 Sep 2007. Horizontal line (dashed–dotted) is diagnosed SBL depth h_d.

vertical velocities, and submeso fluctuations such as downslope winds and intermittent turbulence entering the SBL from aloft (Vickers and Mahrt 2004). Here, to simplify external comparisons between the model and observations, we will diagnose SBL depth in most cases as h_d, the level where the curvature of the thermal profile first reaches a maximum, generally at the top of the strong surface-based nocturnal inversion. However, we note that internally, WRF determines the SBL depth h_m directly from the TKE profile predicted by the MYJ turbulence scheme.

In another diagnostic method, Vickers and Mahrt (2004) found that the buoyancy flux profile can provide a reasonable estimate of SBL depth, at least for undisturbed cases. They found that generally, BF in the SBL is strongly negative at the surface, with its absolute value decreasing almost linearly with height, approaching zero in the thermal residual layer. However, if the layers above the SBL are weakly stable, the BF may remain nonzero or even grow slightly with height. Comparing BF with flux measurements of vertical velocity variance, Vickers and Mahrt (2004) found that SBL depth in the undisturbed case is well correlated with the level where the BF first approaches zero and/or becomes quasi-steady with height. In some cases, this method proved useful for the present study in the first few hours following sunset. Exceptions can occur, especially later during the night. For example, when turbulence develops above an intervening quiescent layer because of wave breaking or shear in a low-level jet (Newsom and Banta 2003; Banta et al. 2007), it can be transported downward, disrupting the ''equilibrium'' SBL structure. Such cases are referred to as intermittently turbulent boundary layers (Mahrt 1998; Van de Wiel et al. 2003; Steeneveld et al. 2006) or ''upside down'' boundary layers (Mahrt and Vickers (2002), in which turbulent episodes may last anywhere from a few

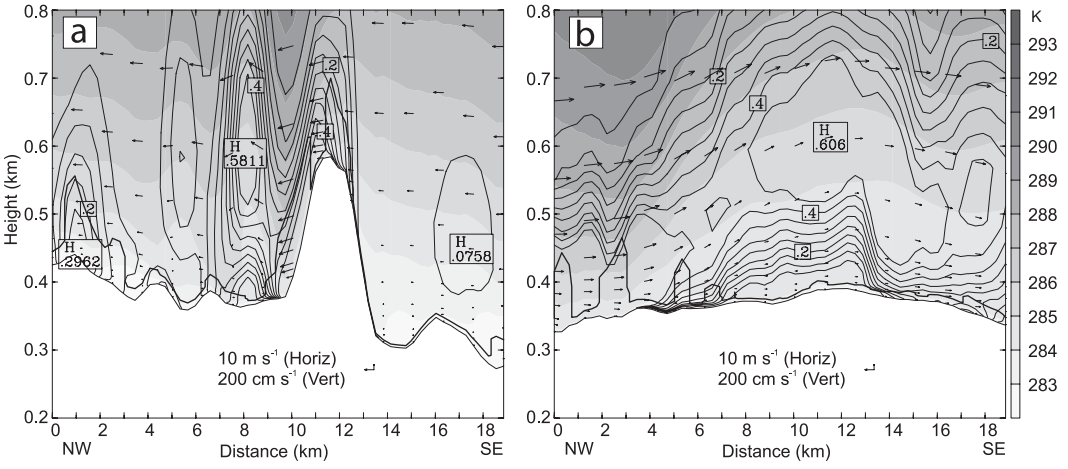

FIG. 9. Predicted potential temperature (gray shades; contour interval 1 K) and TKE (thin solid lines; contour interval 0.05 $m^2 s^{-2}$) vs height (km MSL) in 0.444-km domain at 0936 UTC 14 Nov 2007, along vertical cross sections oriented (a) northwest–southeast and (b) southwest–northeast through Rock Springs in Nittany Valley. Heavy solid line indicates diagnosed SBL depth h_d. Cross section locations are shown in Fig. 2.

minutes to perhaps an hour or so. In these cases SBL depth can be more difficult to define.

1) VERTICAL STRUCTURE OF THE MODELED SBL

Evaluation of ARW-WRF solutions on the 0.444-km inner grid begins with an examination of the early evening vertical structure of the nocturnal SBL at Rock Springs in Experiment Baseline. Figure 8 shows typical early evening profiles predicted by ARW-WRF in the lowest 100 m for four variables at site 3 at 0200 UTC 10 September 2007. The potential temperature (θ) profile in Fig. 8a exhibits a very stable lapse rate of $\Gamma \sim 0.07°C\ m^{-1}$ below 10 m, while maximum curvature appears near 25 m AGL. Meanwhile, the predicted BF profile in Fig. 8b has the characteristic quasi-linear slope up to ~28 m, as observed by Vickers and Mahrt (2004) for undisturbed conditions, and then approaches a near-constant value farther aloft. Near this level, a weak LLJ is found in the speed profile (Fig. 8c). Also note that Fig. 8d reveals a minimum in the Richardson number at or slightly above the same level. Therefore, to be consistent with the BF, Richardson number, and speed profiles, the SBL depth has been diagnosed as $h_d = 28$ m in this case, slightly above the level of maximum curvature of potential temperature. At this same time, the MYJ turbulence scheme in ARW-WRF predicted $h_m \sim 4$–18 m at grid points around Rock Springs, based on its TKE field.

Later that same night the BF profile became more erratic as nonsteady submeso fluctuations developed in the model, making BF less suitable for diagnosing h_d. The θ-curvature and SBL speed maximum usually remained consistent with each other (not shown), but not all profiles exhibited a low-level speed maximum. Thus, as mentioned above, the θ-curvature was preferred for routinely diagnosing h_d when comparing modeled and observed SBL depths.

For the 10 September case the predicted wind direction below h_d at 0200 UTC is north-northeasterly (not shown), with speeds in the SBL of only 0.7–1.7 m s^{-1}. Strong directional shear exists near h_d, with east-southeasterly winds prevailing in the less intense stable layer ($\Gamma \sim 0.01°C\ m^{-1}$) between h_d and 250 m AGL. This deep cool layer forms in part by the pooling of gravity-driven downslope winds from the flanks of the nearby ridges that override the colder SBL below. Farther aloft, a nearly adiabatic residual layer persists above 250 m AGL through the evening, representing the remnants of the daytime convective PBL. As night progresses, h_d remains 25 ~ 35 m deep, while the stable region aloft continues to deepen, eventually filling the entire valley (not shown). Once the stable layer extends up to and above the ridges, mountain waves and transient internal gravity waves can form, which can potentially interact with the low-level SBL (Poulos et al. 2000, 2007; Young et al. 2009). A detailed comparison of model-predicted and observed profiles in the SBL at Rock Springs will be presented below in section 4d as part of the sensitivity experiment evaluations.

Further insights into some typical vertical structures predicted in the high-resolution Baseline Experiment are evident by examining θ and TKE along two 19-km vertical cross sections in Nittany Valley oriented quasi-perpendicular and quasi-parallel to Tussey Ridge (Figs. 2, 9). In this prefrontal cool-season case at 0936 UTC 14 November 2007, strongly sheared southwesterly flow exists over central PA ahead of a small midtropospheric

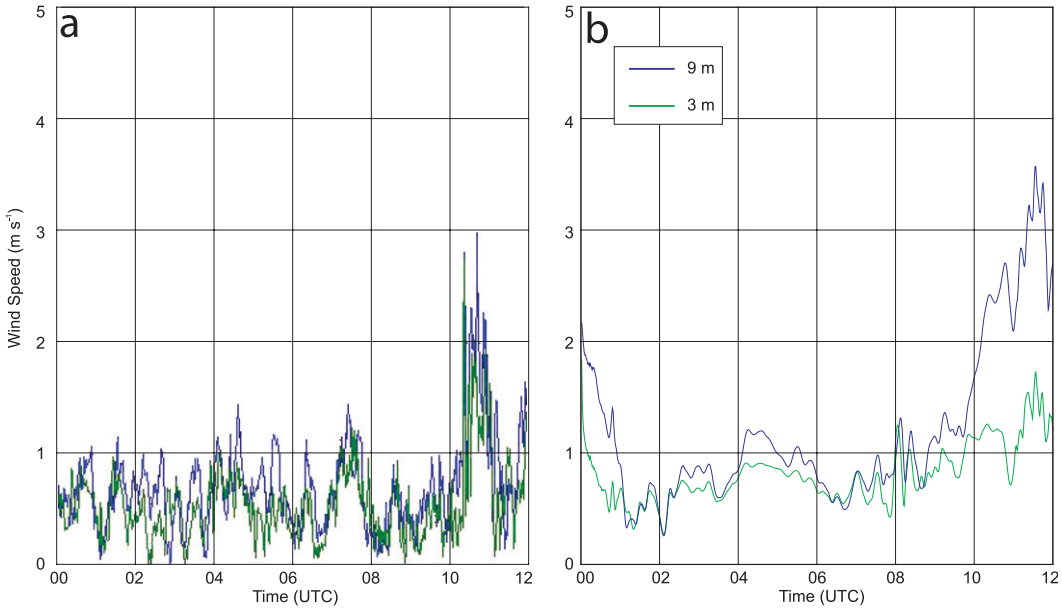

FIG. 10. Vector wind speed (m s^{-1}) at Rock Springs at 0000–1200 UTC 7 Oct 2007: (a) observed 1-min winds from site 3 at 3 m (green) and nearby site 1 at 9 m (blue) AGL and (b) forecasted 1-min winds in Expt Baseline on 0.444-km domain at the same levels.

shortwave advancing from the Ohio Valley. Mean wind near the ridge tops (600 ~ 700 m MSL) is south-southwesterly at 8–12 m s^{-1}, with a small wind component directed across Tussey Ridge from right to left in the northwest–southeast cross section (Fig. 9a). Figures 9a,b show a generally shallow nocturnal SBL diagnosed at h_d ~ 10–30 m, especially at lower elevations, with some lesser regions where h_d ~ 80–100 m, mostly over Tussey

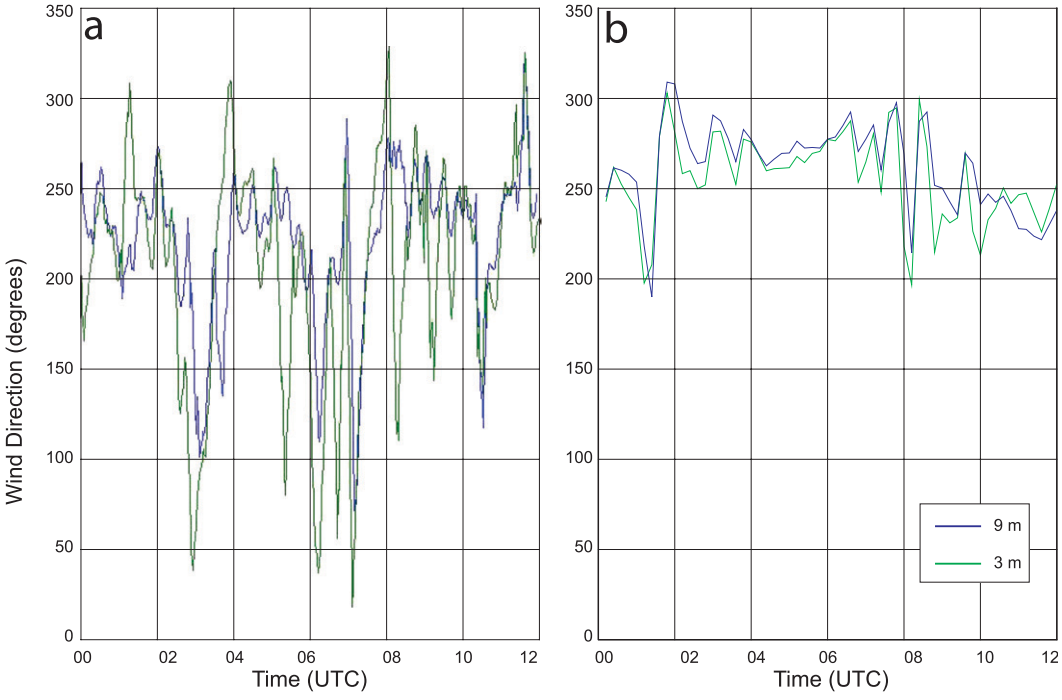

FIG. 11. As in Fig. 10, but for observed and model-predicted near-surface wind direction (°) based on 12-min averages at 0000–1200 UTC 7 Oct 2007.

Ridge and the minor ridges in Nittany Valley. The wind shear aloft generates TKE ~ 0.6 m^2 s^{-2} near the ridge level. Figure 9a shows a group of terrain-induced gravity waves in the northwest–southeast cross section locked into the ridge positions. The other cross section, oriented southwest–northeast along the lowest elevations in Nittany Valley (Fig. 9b), shows that the TKE is very weak near the surface in most of the cold pool (4–19 km on the abscissa). Thus, through most of the night a quiescent layer exists between the shallow SBL in the valley and the shear-induced turbulence aloft, as described by Banta et al. (2007). However, vertical transport of TKE, especially beneath the strongest gravity waves, occasionally leads to intermittent episodes in which the turbulence becomes continuous down to the surface (Banta et al. 2002; Steeneveld et al. 2006). This temporarily establishes a deep upside down SBL (Mahrt and Vickers 2002). Figure 9b shows that this is occurring in the leftmost 4 km of the cross section at 0936 UTC. At other times, when the shear aloft decreases sufficiently in response to mixing or the gravity waves realign in response to changes in the mean wind direction across the terrain, the enhanced TKE tends to weaken and the shallow detached SBL is reestablished along the entire southwest–northeast cross section. Thus, at least qualitatively, the standard MYJ scheme in Experiment Baseline appears quite effective in simulating anticipated SBL structure and the intermittent character of turbulent episodes typical of many nocturnal stable cases where elevated shear exists.

2) TIME SERIES IN THE SBL

Next, examples of time series for observed and modeled wind speed and direction in the SBL are compared at site 3 for 7 October 2007 (Figs. 10, 11).[4] A typical shallow SBL developed on this night under mostly clear skies and weak westerly winds. Consistent with analyses of weakly forced nocturnal conditions by Mahrt (2009) and Mahrt et al. (2010), the observed time series (Figs. 10a, 11a) exhibit large-amplitude high-frequency submeso fluctuations at both 3 and 9 m AGL. For the same period, model solutions on the 0.444-km grid in Experiment Baseline (Figs. 10b, 11b) contain less energy in the highest submeso frequencies, although the variability at somewhat lower frequencies (~20 min or longer) often approaches observed levels. As expected, wind speeds are generally somewhat greater at the 9-m level than at 3 m in both the measurements and the model. Notice that the large rapid fluctuations in the data can make conventional model evaluation methods based on a single time step at 1-h intervals quite problematic. In response, when verifying predicted wind directions, many investigators omit events having speeds less than 1 m s^{-1}. However, it is these weak-wind stable conditions in particular that often present the most urgent forecast problem for plume transport and dispersion applications in the SBL.

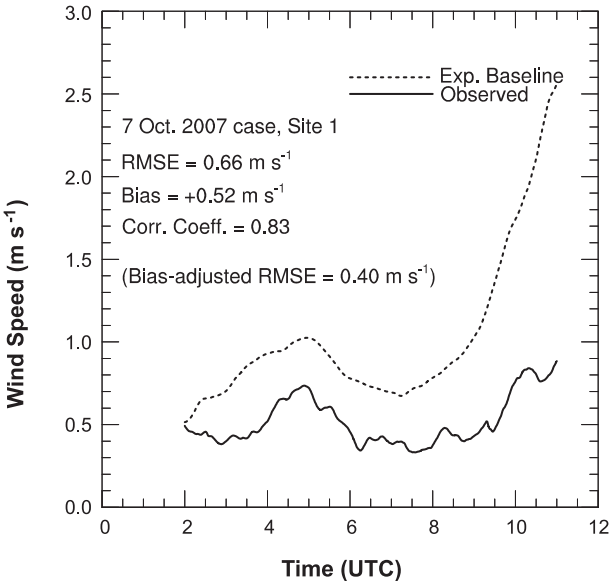

FIG. 12. Filtered deterministic component of vector wind speed (m s^{-1}) at site 1 (9 m AGL) on the 0.444-km domain at 0200–1100 UTC 7 Oct 2007 for Expt Baseline (dashed line) vs observations (solid line).

The speeds and directions shown in Figs. 10, 11 are based on 1- and 12-min averaged data, respectively.[5] These frequencies are too low to be explained by 3D turbulence in the SBL and have been described by Mahrt et al. (2010) as nonturbulent submeso motions of uncertain origin, possibly due to transient internal gravity waves or intermittency in the downslope drainage flow. Gaudet et al. (2008) show that wind fluctuations in the submeso range (1 ~ 20 min) are effectively nondeterministic, while lower frequencies in subkilometer ARW-WRF solutions may be predictable, at least in part. Thus, a 2-h running-mean filter can be applied to the winds to isolate the lower-frequency deterministic components in the time series, such as the general increase of speed in the final hours before sunrise.

Figure 12 shows an example of the filtered time series winds in Experiment Baseline at 9 m for 7 October 2007. The filtering step removes brief submeso gusty episodes, revealing a fairly strong correlation between modeled

[4] On 7 October, sunset at Rock Springs occurs at 2245 UTC (1745 LST) and sunrise at 1114 UTC (0614 LST).

[5] The raw time series data for wind direction are actually based on 1-min averages, but are shown here as 12-min averages simply for better legibility.

TABLE 4. Statistics for filtered wind speed, direction, and temperature errors at Rock Springs at site 1 (9 m AGL) on the 0.444-km domain for Expt Baseline, based on 32 nocturnal SBL cases in October–November 2007 and June 2008.

Variable	RMSE	Bias error	Bias-corrected RMSE	Mean absolute error (direction)	Obs mean
Wind speed (m s^{-1})	1.15	0.64	0.69	—	0.84
Wind direction (°) (0.5 m s^{-1} threshold)	39.6	−4.6	—	27.7	231.8
Wind direction (°) (0.1 m s^{-1} threshold)	57.4	2.6	—	41.4	227.4
Temperature (°C)	2.9	1.4	1.4	—	12.7

and observed wind variability on times scales down to 20–30 min (cf. Fig. 10). Despite very weak mean flow in the SBL, standard statistical measures (RMSE, bias error, correlation coefficient, and bias-corrected RMSE) calculated from the filtered series[6] confirm that wind speeds predicted on the 0.444-km domain in Experiment Baseline have considerable skill. While the figure reveals a positive bias of ~0.5 m s^{-1} for this case, the correlation coefficient is 0.83 and RMSE is 0.66 m s^{-1}. Since the bias-corrected RMSE is only 0.40 m s^{-1}, much of the RMSE is systematic. This is potentially important because systematic biases may imply correctable model errors, perhaps in a physics parameterization.

In addition to the general positive speed bias, Fig. 12 also reveals a substantial increase of the winds in the final 2 h of the forecast period, especially in the model, leading to a maximum forecast error of 1.7 m s^{-1} at 1130 UTC. Further analysis of the model predictions for this case by Young et al. (2009) suggests that the probable cause of the acceleration near the end of the period was due to downward vertical transport of momentum following gravity wave breaking near the level of the ridge tops. Although no observations are available aloft to confirm this hypothesis, similar (but weaker) near-surface accelerations of the submeso speed fluctuations in the data suggest similar mechanisms are likely at work (Figs. 10a,b). However, while the observed wind increases are nearly the same at 3 and 9 m, acceleration in the model solution is strongly exaggerated at 9 m. The reason why the spurious acceleration is found primarily at 9 m is not entirely clear, but it is noted that the model's nocturnal cold pool was weaker than observed, which may have allowed momentum from aloft to penetrate more easily into the most stable layers.

The time filter was applied subsequently to observed and modeled time series taken from 32 mostly clear autumn and spring cases that satisfied the SBL case selection criteria described earlier. For 95% of the nocturnal hours in these cases, observed wind speeds at the nearest METAR station, SCE, were 3 m s^{-1} or less, with only 1% of hours exceeding 5 m s^{-1}. Table 4 summarizes the 32-case average statistics calculated for wind speed, direction, and temperature errors for Experiment Baseline at site 1 (9 m AGL) in the local Rock Springs network. As for the single case of 7 October 2007, the table reveals a small positive speed bias (+0.64 m s^{-1}) in the nocturnal SBL, along with an average warm temperature bias of +1.4 K. Similar positive biases were found at the 3-m level, and examination of the temporal behavior of the biases indicates that, while observed SBL temperatures and wind speeds tend to decrease steadily through the night, the ARW-WRF model's predicted cooling rate is about half that observed, while predicted speed remains almost constant in time (not shown). These errors are consistent with possibly excessive background (minimum) mixing in the cold pool by the standard MYJ turbulence scheme, as hypothesized in section 2c. A weakened cold pool can also explain why the sign of the surface temperature bias in the valley (Table 4) is opposite to that in the two coarse domains (Table 3).

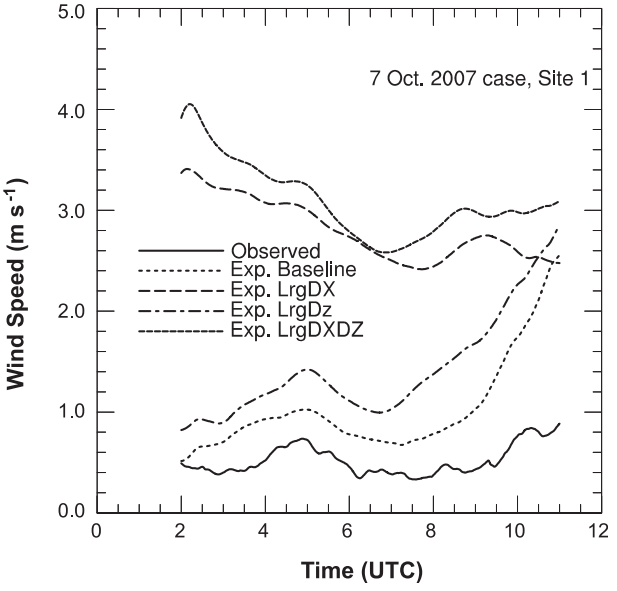

FIG. 13. Sensitivity of filtered deterministic components of vector wind speed (m s^{-1}) to horizontal and vertical resolution at site 1, 9 m AGL at 0200–1100 UTC 7 Oct 2007. Shown are model-predicted speeds in Expt Baseline (dotted line), Expt LrgDX (long dashed line), Expt LrgDZ (dashed–dotted line), and Expt LrgDXDZ (short dashed line). Observed speed (filtered; m s^{-1}) shown as solid line.

[6] A 30-min sampling interval was used when calculating statistics for the nocturnal time series.

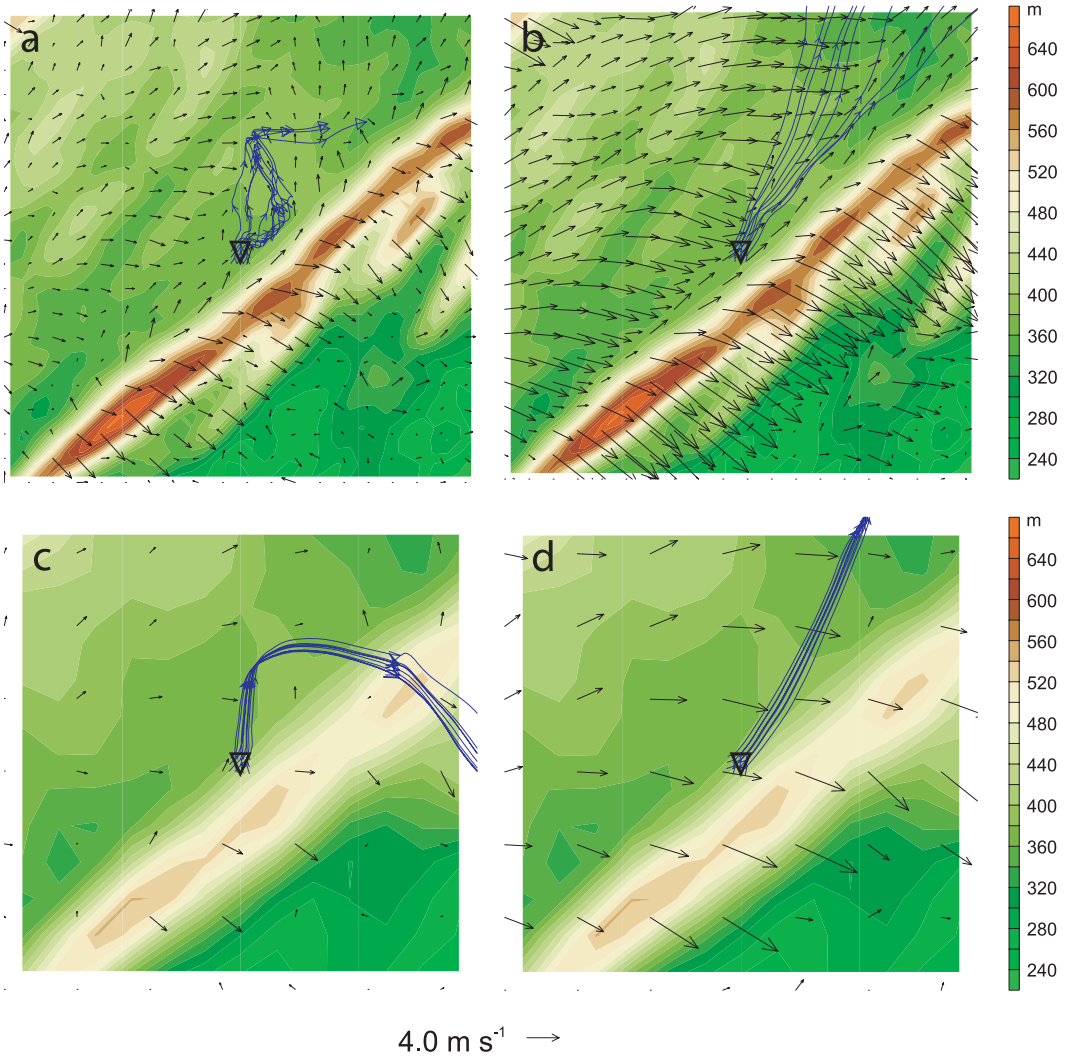

FIG. 14. Predicted parcel trajectories at 0800–1112 UTC (blue) and wind vectors at every other grid point at 1112 UTC at the lowest model level in a subregion (see Fig. 2) in the vicinity of Rock Springs on 7 Oct 2007. Nine parcels were released at 3 m AGL in a 0.444 km × 0.444 km area denoted by ▼ at 0800 UTC. Results are for (a) Expt Baseline, (b) Expt LrgDZ, (c) Expt LrgDX, and (d) Expt LrgDXDZ. Terrain (m) is shown as color fill.

Note that because the average observed nocturnal speeds in the SBL at Rock Springs were less than 1 m s^{-1}, most of the wind samples would have been rejected if a standard minimum speed threshold of 1.0 m s^{-1} had been used when calculating direction errors. This would have caused the resulting error statistics for direction to be unrepresentative of the weakly forced cases of greatest interest. However, because the Rock Springs measurements were made using sensitive sonic anemometers accurate at much slower speeds than more common propeller-and-vane anemometers, it became practical to calculate statistics based on lower thresholds of 0.5 and 0.1 m s^{-1}. Despite including such very light winds in the calculations, Table 4 shows that the model-predicted direction errors are similar to those found in Table 3 and many other modeling studies where larger speed thresholds of 1–2 m s^{-1} were imposed (e.g., Schroeder et al. 2006; Mass et al. 2002). Also, RMSEs for the filtered wind speeds were much smaller than those often reported in the literature, as well as reported for unfiltered winds on the 12- and 4-km ARW-WRF domains (Table 3). In most cases the filtering step reduced errors in speed, direction, and temperature by ~25%–50%. These results demonstrate that the ARW-WRF model in Experiment Baseline has considerable skill for predicting speed, direction, and temperature in weakly forced nocturnal SBLs, and may have the potential for even better accuracy if systematic biases can be identified and corrected.

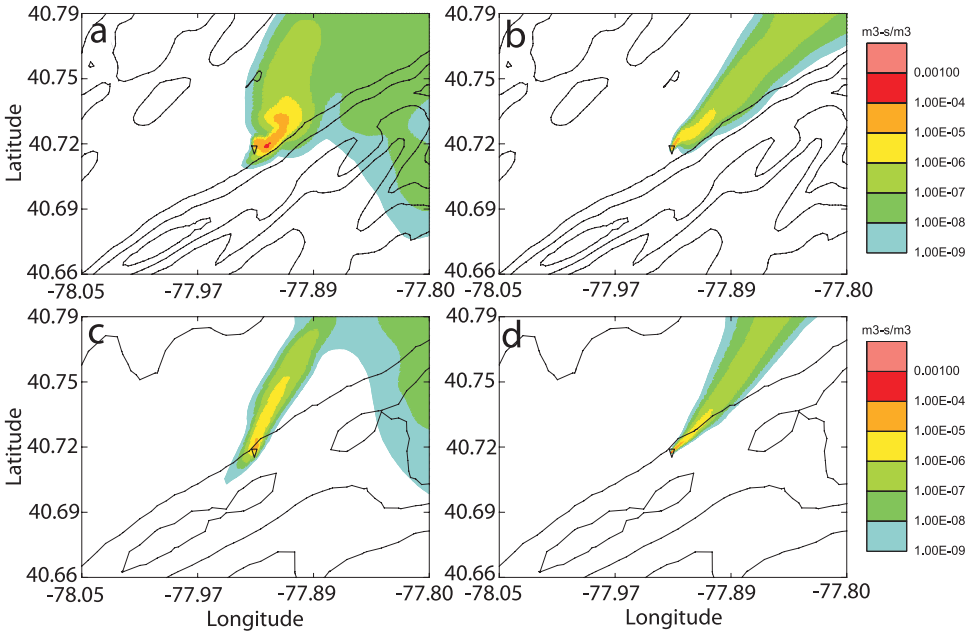

FIG. 15. SCIPUFF surface plume dosages calculated using ARW-WRF–predicted meteorology on a small subregion in the vicinity of Rock Springs at 0800–1112 UTC 7 Oct 2007. Results are for (a) Expt Baseline, (b) Expt LrgDZ, (c) Expt LrgDX, and (d) Expt LrgDXDZ. Dosage (m^3 s m^{-3}) is shown as color fill.

c. *Sensitivity to grid resolution*

The dependence of model-predicted wind speed on horizontal and vertical resolution over moderately inhomogeneous terrain was explored next by comparing Experiment Baseline to the three grid-sensitivity experiments: LrgDZ, LrgDX, and LrgDXDZ. A typical example is shown in Fig. 13 for 7 October 2007. Clearly, Experiment Baseline produces the most accurate speeds despite a bias of about +0.5 m s^{-1}. In Experiment LrgDZ, the case-averaged bias is ~+0.9 m s^{-1}, although the trend is generally well correlated with Experiment Baseline and the observations. However, in both Experiments LrgDX and LrgDXDZ, the positive biases are much larger, approaching +3 m s^{-1}, and predicted trends are significantly different than observed. Thus, both high horizontal and vertical resolution can be important for ensuring model accuracy in the weakly forced nocturnal SBL, and it appears that solutions are particularly sensitive to horizontal resolution, emphasizing the importance of resolving subkilometer complex terrain in stable conditions.

Speed errors, of course, are not the only model errors affecting plume transport and dispersion calculations in the SBL. Errors in predicted low-level stability, vertical motions, and wind direction can be equally important. Sensitivity to the integrated effects of meteorological errors on transport was examined by computing particle trajectories based on ARW-WRF's 3D wind fields, again using the 7 October 2007 case (Fig. 14). The trajectories are based on the unfiltered model wind fields saved at 12-min intervals. For each experiment, nine parcels were released at 0800 UTC from 3 m AGL at regular 222-m spacing within a single 0.444-km grid cell at Rock Springs. The figure reveals very different trajectories over the period 0800–1112 UTC entirely due to changes in horizontal and vertical resolution. Trajectories in Experiment Baseline (Fig. 14a) exhibit moderate divergence due to submeso speed and direction fluctuations (Figs. 10b, 11b), resulting in gentle meandering of the particle cluster. All particles in Experiment Baseline remain trapped below 30 m AGL in the very stable air near the valley floor throughout the 3-h period.

In the other three experiments, however, the particles experience differing degrees of weaker low-level stability and faster speeds following their release, often resulting in lofting to heights of 50–100 m AGL. At these heights, winds were generally faster than those near the surface and directions were often quite different, resulting in very dissimilar trajectories compared to Experiment Baseline. Thus, particles in Experiment LrgDZ (Fig. 14b) experience virtually no meandering. Instead they slowly diverge over a 25° arc while traveling rapidly to the northeast out of the subdomain. In this experiment, the coarse model layers near the surface (Fig. 3b) tend to weaken the downslope drainage flow and submeso variability largely responsible for plume meandering. Meanwhile, several

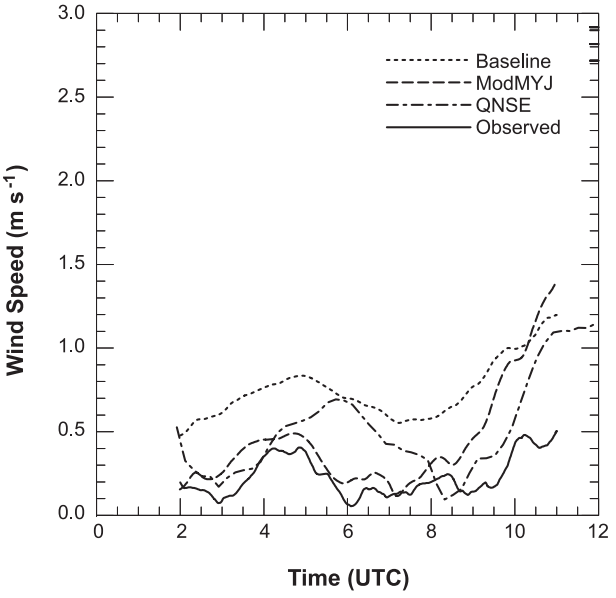

FIG. 16. Filtered vector wind speed (m s^{-1}) at site 3 (3 m AGL) at 0200–1100 UTC 7 Oct 2007 as a function of turbulence scheme. Shown are model-predicted winds on the 444-m domain for Expt Baseline (dotted line; standard MYJ), Expt ModMYJ (dashed line), and Expt QNSE (dashed–dotted line). Observed filtered speed (m s^{-1}) shown as solid curve.

other factors combine in Experiments LrgDX and LrgDXDZ to make different particle trajectories from those predicted in Experiment Baseline. First, similar to Experiment LrgDZ, the coarse *horizontal* resolution in these two final sensitivity experiments tended to suppress particle divergence because of poor representation of submeso wind variability. The coarser grid also caused the narrow ridges to be poorly resolved, reducing their blocking and channeling effects in a stable environment. This is especially evident in Experiment LrgDX (Fig. 14c), where the particles cross an "eroded" Tussey Ridge and quickly exit the subdomain toward the southeast. Finally, a very strong positive speed bias is evident in Experiment LrgDXDZ (Fig. 14d), causing all particles to exit the subdomain toward the northeast long before they can experience a dramatic change of wind direction in the final hour of the trajectory test period.

Figure 15 shows the corresponding surface plume dosages calculated using the Second-Order Closure Integrated Puff (SCIPUFF) AT&D model of Sykes et al. (1993, 1998), based on the meteorological fields from the four ARW-WRF resolution-sensitivity experiments. The figure reveals that the faster speeds and absence of submeso variability associated with reducing grid resolution in either the horizontal or vertical direction result in greater ventilation, narrower plumes, and significantly lower maximum surface dosages. The Baseline Experiment, with its strong stability and weak meandering submeso flow, produced a wider plume and locally higher dosages by as much as two orders of magnitude in the vicinity of Rock Springs. While no tracer measurements were available to verify the model-generated plumes, the more accurate speeds detected at Rock Springs and the tendency for particles to remain trapped within the shallow nocturnal cold pool in Experiment Baseline appear to be mostly consistent with expected plume behavior in the SBL. These results further confirm the importance of very fine grid resolution when predicting transport and dispersion by weakly forced flow in complex terrain and very stable conditions.

TABLE 5. Sensitivity of filtered wind speed to turbulence parameterization at Rock Springs at site 1 (3 m AGL) on the 0.444-km domain for the case of 7 Oct 2007.

Expt	RMSE (m s^{-1})	Bias error (m s^{-1})	Correlation coefficient
Expt Baseline	0.52	0.51	0.78
Expt ModMYJ	0.33	0.22	0.80
Expt QNSE	0.30	0.23	0.59

d. Sensitivity to modeled subgrid turbulence in stable conditions

Table 4 revealed a positive bias in the 32-case average near-surface wind speed for Experiment Baseline despite very fine grid resolution. This is consistent with the hypothesis in section 2b that the values of minimum background TKE_{MIN} and l_b in the standard MYJ turbulence scheme may force excessive mixing in very stable conditions. Again using the test case of 7 October 2007, Experiments ModMYJ and QNSE were compared to Experiment Baseline (Fig. 16) to test whether two alternative turbulence formulations may help reduce the positive speed biases in the lower levels for stable conditions, where the background mixing is expected to have its greatest spurious effect. The figure shows that the two alternative schemes do tend to reduce the 3-m wind speed by ~0.3 m s^{-1}, except perhaps in the final 1–2 h of the night. This results in smaller averaged RMSEs and biases, compared to Experiment Baseline (Table 5). The table also shows that correlation with the observations remains quite high, especially for Experiment ModMYJ, suggesting that the physical processes most responsible for submeso motions in this case were barely affected by the changes in the turbulence schemes and therefore were probably initiated at some distance from site 1.

Additional tests performed using an independent case, 5 September 2009, confirm that 3-m θ and wind speed are reduced in the shallow SBL for both Experiments ModMYJ and QNSE, compared to the Baseline Experiment.

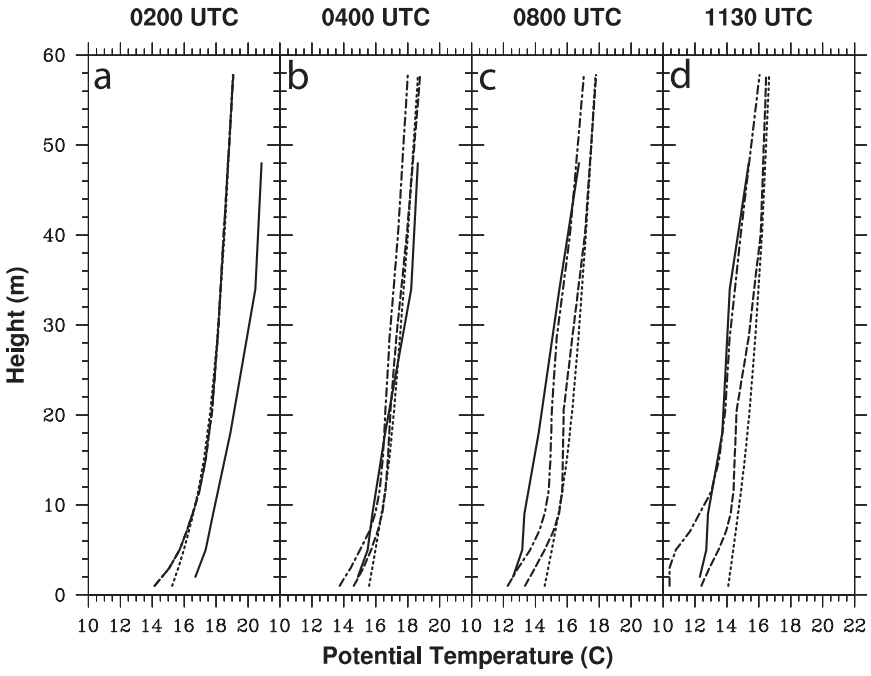

FIG. 17. Vertical profiles of 30-min averaged potential temperature (°C) in the lowest 50 m AGL at Rock Springs on 5 Sep 2009. Profiles shown are observed (solid line), Expt Baseline (dotted line), Expt ModMYJ (dashed line), and Expt QNSE (dashed–dotted line) at (a) 0200, (b) 0400, (c) 0800, and (d) 1130 UTC. Observed θ profiles are a composite of data at sites 1 and 10. Modeled θ shown at site 1.

However, vertical profiles in the lowest 50 m reveal that the impact of the smaller background parameters is minimal above 10 m, approximately the depth of the SBL, for Experiment ModMYJ (Figs. 17, 18). Although Experiment QNSE shows results similar to Experiment ModMYJ below 10–15 m, it produces larger differences above 15 m. It is evident that smaller background turbulence parameters in these alternative schemes produce stronger surface-based inversions and greater wind shear in the shallow SBL. Of course, the positive biases found in Experiment Baseline may also be caused in part by possible systematic errors in other model components, such as the initial conditions, roughness formulations, and canopy or radiation physics. Further testing with a wider variety of cases is needed to better understand the overall impact on model accuracy of these formulations. However, these experiments indicate that minor modifications to the MYJ scheme, or switching to the QNSE scheme, can intensify low-level vertical gradients, as often observed in weakly forced, very stable nocturnal cases.

Last, the sensitivity of particle trajectories in the SBL to the two alternative turbulence schemes is shown for 7 October 2007 (Fig. 19). As in section 4c, nine particles were released from 3 m AGL at 0800 UTC in a single grid cell. In Experiment ModMYJ, the reduced mean wind speed and greater near-surface stability allowed the submeso direction fluctuations in the cold pool to have a larger impact, leading to more dispersive particle meandering in the model (cf. Figs. 14a, 19a). However, Fig. 19b reveals that even though Experiment QNSE also had slower low-level mean wind speeds, the meandering particles traveled more rapidly, with several of them quickly escaping the Nittany Valley. This behavior occurs because most particles in Experiment QNSE were lofted above the shallow SBL in the first hour after their release, where they then followed a helical path toward the northeast between ~50 and 200 m AGL, generally parallel to Tussey Ridge (not shown). The particles experienced faster winds in these layers than in the SBL and some were carried quite rapidly across the ridge. While it is not entirely clear why more vigorous lofting of particles occurred in Experiment QNSE than in Experiment ModMYJ, despite strong surface inversions in both, it is possible that the low-level SBL flow and vertical motions associated with the passage of transient internal gravity waves may have phased more advantageously in the QNSE Experiment. These results demonstrate that extremely complex interactions between submeso motions in stable conditions, forced by a variety of poorly understood physical processes, can easily lead to dramatically different hazard predictions.

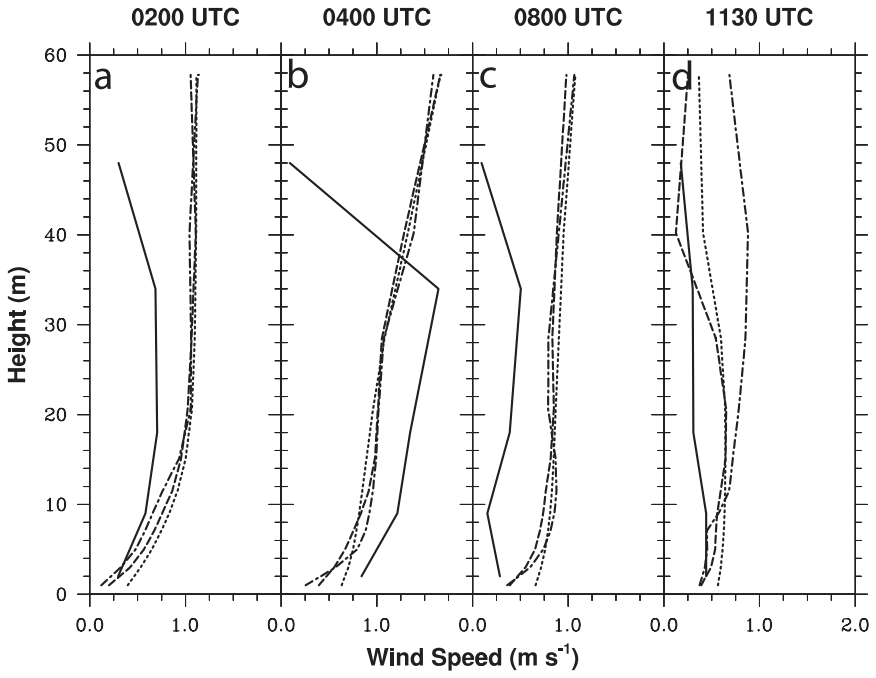

FIG. 18. Vertical profiles of 30-min averaged wind speed (m s^{-1}) in the lowest 50 m AGL at Rock Springs on 5 Sep 2009. Profiles shown are observed (solid line), Expt Baseline (dotted line), Expt ModMYJ (dashed line), and Expt QNSE (dashed–dotted line) at (a) 0200, (b) 0400, (c) 0800, and (d) 1130 UTC. Observed wind profiles are a composite of data at sites 1 and 10. Modeled winds shown at site 1.

5. Summary

In this study, a version of the ARW-WRF meteorological prediction model utilizing subkilometer grid spacing and a small instrumented field network were used to study predictability in weakly forced nocturnal SBL conditions in moderately complex topography. It has been shown that the modeling system, with the standard MYJ turbulence scheme, can predict important aspects of the nocturnal SBL, including realistic buoyancy flux profiles, intermittent LLJ turbulence, submeso fluctuations in wind speed and direction, and low-level stable meandering.

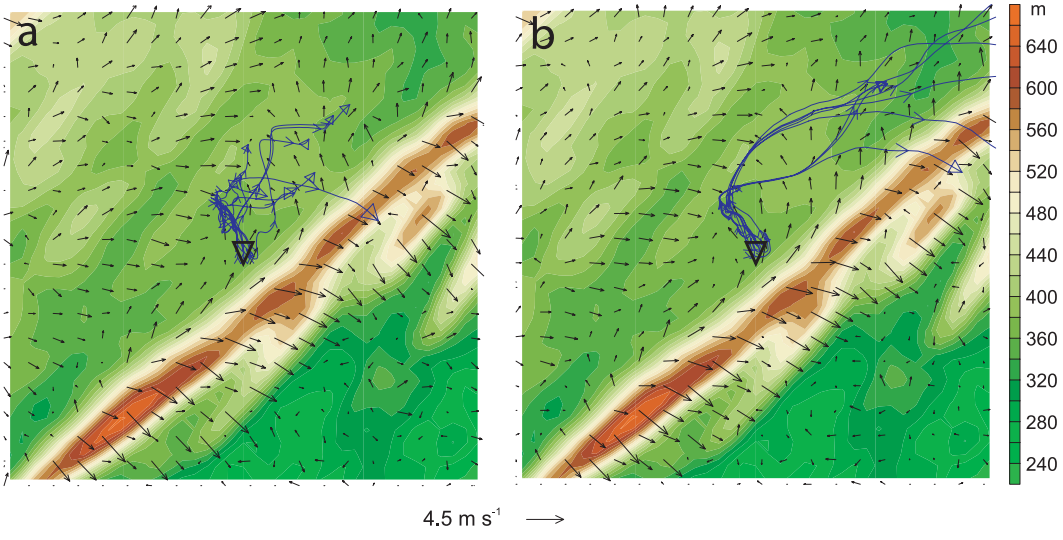

FIG. 19. As in Fig. 14, but for (a) Expt ModMYJ and (b) Expt QNSE.

Subkilometer horizontal resolution and very fine vertical resolution in the SBL were found to be important for predicting nocturnal wind speeds in weakly forced situations. However, the default background minima for TKE and turbulent length scale in the standard MYJ scheme appeared large enough to contribute to possible excessive mixing in very stable conditions, which can contribute to positive biases in speed and temperature below 10 m. Simple modifications to the MYJ and QNSE schemes can significantly reduce these biases, at least near the surface. Predicted nocturnal winds on time scales of ~20 min or longer were found to contain speed and direction fluctuations that are fairly consistent with submeso fluctuations observed in the valley cold pool. These fluctuations are thought to be related to fluctuating drainage winds, transient internal gravity waves, and intermittent shear-induced mixing of momentum in the LLJ. Statistical accuracy of the model solutions at these scales is best revealed by filtering out the nondeterministic higher-frequency fluctuations from observed and predicted time series.

This work emphasizes the large sensitivity of transport and dispersion solutions in the SBL implied by different model-dependent factors such as grid resolution and turbulence physics, and the potential advantage of an ensemble modeling approach to transport and dispersion predictions (e.g., Kolczynski et al. 2009). Even finer resolution might enable a model to more accurately simulate interactions between transient wave phenomena and strong low-level stability, which appears to generate much of the submeso variability in the SBL. Other factors, including initial conditions and various aspects of the model physics, are likely to contribute to forecast uncertainty. Much additional work is needed to evaluate very finescale model predictions in very stable nocturnal conditions for different topographic regimes. The field network in central PA is currently being enhanced to provide remotely sensed winds through at least 200 m AGL, which will help advance our understanding of the interactions between terrain-induced gravity waves, LLJ turbulence, drainage winds, and the valley cold pool.

Acknowledgments. This project received support from the Defense Threat Reduction Agency (DTRA)–Joint Science and Technology Office for Chemical and Biological Defense (Contract W911NF-06-1-0439-MOD-P00001 and Grant HDTRA1-10-1-0033). DTRA also provided DTED-1 high-resolution terrain data over central PA. Dr. Aijun Deng of Penn State assisted with applications of the SCIPUFF model and adapted the DTRA terrain data for WRF's subkilometer domain. Dr. Zavisa Janjic of the National Centers for Atmospheric Prediction provided many valuable insights into the MYJ turbulence physics. Dr. Boris Galperin of the University of South Florida gave helpful guidance on the QNSE turbulence scheme. Karen Tinklepaugh of Penn State assisted with the figures.

REFERENCES

Andre, J. C., and L. Mahrt, 1982: The nocturnal surface inversion and influence of clear-air radiative cooling. *J. Atmos. Sci.,* **39,** 864–878.

Anfossi, D., D. Oettl, G. Degrazia, and A. Goulart, 2005: An analysis of sonic anemometer observations in low wind speed conditions. *Bound.-Layer Meteor.,* **114,** 179–203.

Banta, R. M., R. K. Newsom, J. K. Lundquist, Y. L. Pichugina, R. L. Coulter, and L. Mahrt, 2002: Nocturnal low-level jet characteristics over Kansas during CASES-99. *Bound.-Layer Meteor.,* **105,** 221–252.

——, L. Mahrt, D. Vickers, J. Sun, B. B. Balsley, Y. L. Pichugina, and E. J. Williams, 2007: The very stable boundary layer on nights with weak low-level jets. *J. Atmos. Sci.,* **64,** 3068–3090.

Belusic, D., and L. Mahrt, 2008: Estimation of length scales from mesoscale networks. *Tellus,* **60A,** 706–715.

Bravo, M., T. Mira, M. R. Soler, and J. Cuxart, 2008: Intercomparison and evaluation of MM5 and Meso-NH mesoscale models in the stable boundary layer. *Bound.-Layer Meteor.,* **128,** 77–101.

Brost, R. A., and J. C. Wyngaard, 1978: A model study of the stably stratified planetary boundary layer. *J. Atmos. Sci.,* **35,** 1427–1440.

Chen, F., and J. Dudhia, 2001a: Coupling of an advanced land surface–hydrology model with the Penn State–NCAR MM5 modeling system. Part I: Model implementation and sensitivity. *Mon. Wea. Rev.,* **129,** 569–585.

——, and ——, 2001b: Coupling of an advanced land surface–hydrology model with the Penn State–NCAR MM5 modeling system. Part II: Preliminary model validation. *Mon. Wea. Rev.,* **129,** 587–604.

Cuxart, J., and M. A. Jimenez, 2007: Mixing processes in a nocturnal low-level jet: An LES study. *J. Atmos. Sci.,* **64,** 1666–1679.

——, and Coauthors, 2006: Single-column model intercomparison for a stably stratified atmospheric boundary layer. *Bound.-Layer Meteor.,* **118,** 273–303.

——, M. A. Jimenez, and D. Martinez, 2007: Nocturnal meso-beta basin and katabatic flows on a midlatitude island. *Mon. Wea. Rev.,* **135,** 918–932.

Dabberdt, W. F., and Coauthors, 2005: Multifunctional mesoscale observing networks. *Bull. Amer. Meteor. Soc.,* **86,** 961–982.

Deng, A., and D. R. Stauffer, 2006: On improving 4-km mesoscale model simulations. *J. Appl. Meteor. Climatol.,* **45,** 361–381.

——, N. L. Seaman, G. K. Hunter, and D. R. Stauffer, 2004: Evaluation of interregional transport using the MM5–SCIPUFF system. *J. Appl. Meteor.,* **43,** 1864–1886.

Dudhia, J., 1989: Numerical study of convection observed during the Winter Monsoon Experiment using a mesoscale two-dimensional model. *J. Atmos. Sci.,* **46,** 3077–3107.

Elmore, K. L., D. J. Stensrud, and K. C. Crawford, 2002: Explicit cloud-scale models for operational forecasts: A note of caution. *Wea. Forecasting,* **17,** 873–884.

Etling, D., 1990: On plume meandering under stable stratification. *Atmos. Environ.,* **8,** 1979–1985.

Fritts, D. C., C. Nappo, D. M. Riggin, B. B. Balsley, W. E. Eichinger, and R. K. Newsom, 2003: Analysis of ducted motions in the

stable nocturnal boundary layer during CASES-99. *J. Atmos. Sci.,* **60,** 2450–2472.

Gaudet, B. J., N. L. Seaman, D. R. Stauffer, S. Richardson, L. Mahrt, and J. C. Wyngaard, 2008: Verification of WRF-predicted mesogamma-scale spectra in the SBL using a high-frequency filter decomposition. Preprints, *Ninth WRF Users' Workshop,* Boulder, CO, NCAR/MMM, P8.1. [Available online at http://www.mmm.ucar.edu/events/2008_wrfusers/index.php.]

Gego, E., C. Hogrefe, G. Kallos, A. Voudouri, J. S. Irwin, and S. T. Rao, 2005: Examination of model predictions at different horizontal grid resolutions. *Environ. Fluid Mech.,* **5,** 63–85.

Grell, G. A., J. Dudhia, and D. R. Stauffer, 1994: A description of the fifth generation Penn State/NCAR mesoscale model (MM5). NCAR Tech. Note NCAR/TN-398+STR, 138 pp. [Available from NCAR Information Support Services, P.O. Box 3000, Boulder, CO 80397.]

Ha, K.-J., and L. Mahrt, 2003: Radiative and turbulent fluxes in the nocturnal boundary layer. *Tellus,* **55A,** 317–327.

Hanna, S. R., 1983: Lateral turbulence intensity and plume meandering during stable conditions. *J. Climate Appl. Meteor.,* **22,** 1424–1430.

Hiscox, A. L., D. R. Miller, and C. J. Nappo, 2010: Plume meander and dispersion in a stable boundary layer. *J. Geophys. Res.,* **115,** D21105, doi:10.1029/2010JD014102.

Holland, L., J. Halley-Gotway, B. Brown, and R. Bullock, 2007: A toolkit for model evaluation. Preprints, *Eighth WRF Users' Workshop,* Boulder, CO, NCAR/MMM, 3.2. [Available online at http://www.mmm.ucar.edu/events/2007_wrfusers/agenda.php.]

Janjic, Z. I., 2002: Nonsingular implementation of the Mellor-Yamada level 2.5 scheme in the NCEP meso model. NCEP Office Note 437, 61 pp. [Available online at http://www.emc.ncep.noaa.gov/officenotes/newernotes/on437.pdf.]

Kain, J. S., and J. M. Fritsch, 1993: Convective parameterization for mesoscale models: The Kain-Fritsch scheme. *The Representation of Cumulus Convection in Numerical Models, Meteor. Monogr.,* No. 46, Amer. Meteor. Soc., 165–170.

——, and ——, 1998: Multiscale convective overturning in mesoscale convective systems: Reconciling observations, simulations, and theory. *Mon. Wea. Rev.,* **126,** 2254–2273.

——, S. J. Weiss, J. J. Levit, M. E. Baldwin, and D. R. Bright, 2006: Examination of convection-allowing configurations of the WRF model for the prediction of severe convective weather: The SPC/NSSL Spring Program 2004. *Wea. Forecasting,* **21,** 167–181.

Kang, S. L., and K. Davis, 2008: The effects of mesoscale surface heterogeneity on the fair-weather convective atmospheric boundary layer. *J. Atmos. Sci.,* **65,** 3197–3213.

Koch, S. E., and R. Gall, 2005: The DTC Winter Forecast Experiment: Final project report. NCAR Rep., 27 pp. [Available from Development Testbed Center, NCAR Research Applications Laboratory, P.O. Box 3000, Boulder, CO 80397.]

Kolczynski, W. C., Jr., D. R. Stauffer, S. E. Haupt, and A. Deng, 2009: Ensemble variance calibration for representing meteorological uncertainty for atmospheric transport and dispersion modeling. *J. Appl. Meteor. Climatol.,* **48,** 2001–2021.

Mahrt, L., 1998: Stratified atmospheric boundary layers and breakdown of models. *Theor. Comput. Fluid Dyn.,* **11,** 263–279.

——, 2007: Weak-wind mesoscale meandering in the nocturnal boundary layer. *Environ. Fluid Mech.,* **7,** 331–347.

——, 2008: Mesoscale wind direction shifts in the stable boundary-layer. *Tellus,* **60A,** 700–705.

——, 2009: Characteristics of submeso winds in the stable boundary layer. *Bound.-Layer Meteor.,* **130,** 1–14.

——, and D. Vickers, 2002: Contrasting vertical structures of nocturnal boundary layers. *Bound.-Layer Meteor.,* **105,** 351–363.

——, and R. Mills, 2009: Horizontal diffusion by submeso motions in the stable boundary layer. *Environ. Fluid Mech.,* **9,** 443–456.

——, J. Sun, W. Blumen, T. Delany, and S. Oncley, 1998: Nocturnal boundary-layer regimes. *Bound.-Layer Meteor.,* **88,** 255–278.

——, C. K. Thomas, and J. H. Prueger, 2009: Space-time structure of mesoscale modes in the stable boundary layer. *Quart. J. Roy. Meteor. Soc.,* **135,** 67–75.

——, S. Richardson, N. Seaman, and D. Stauffer, 2010: Interaction between drainage flows, the valley cold pool and submeso motions. *Tellus,* **62A,** 698–705.

Mass, C. F., D. Ovens, K. Westrick, and B. A. Colle, 2002: Does increasing horizontal resolution produce more skillful forecasts? *Bull. Amer. Meteor. Soc.,* **83,** 407–430.

Mestayer, P. G., and S. Anquetin, 1995: Climatology of cities. *Diffusion and Transport of Pollutants in Atmospheric Mesoscale Flow Fields,* A. Gyr and F.-S. Rys, Eds., Kluwer Academics, 165–189.

Nappo, C., 2002: *An Introduction to Atmospheric Gravity Waves*. Academic Press, 279 pp.

Nastrom, G. D., and K. S. Gage, 1985: A climatology of atmospheric wavenumber spectra of wind and temperature observed by commercial aircraft. *J. Atmos. Sci.,* **42,** 950–960.

Newsom, R. K., and R. M. Banta, 2003: Shear-flow instability in the stable nocturnal boundary layer as observed by Doppler lidar during CASES-99. *J. Atmos. Sci.,* **60,** 16–33.

Poulos, G. S., J. E. Bossert, T. B. McKee, and R. A. Pielke, 2000: The interaction of katabatic flow and mountain waves. Part I: Observations and idealized simulations. *J. Atmos. Sci.,* **57,** 1919–1936.

——, ——, ——, and R. A. Pielke Sr., 2007: The interaction of katabatic flow and mountain waves. Part II: Case study analysis and conceptual model. *J. Atmos. Sci.,* **64,** 1857–1879.

Ralph, F. M., and Coauthors, 2005: Improving short-term (0–48 h) cool-season quantitative precipitation forecasting: Recommendations from a USWRP workshop. *Bull. Amer. Meteor. Soc.,* **86,** 1619–1632.

Reen, B. P., D. R. Stauffer, K. J. Davis, and A. R. Desai, 2006: A case study on the effects of heterogeneous soil moisture on mesoscale boundary-layer structure in the Southern Great Plains, U.S.A. Part II: Mesoscale modeling. *Bound.-Layer Meteor.,* **120,** 275–314.

Rife, D. L., and C. A. Davis, 2005: Verification of temporal variations in mesoscale numerical wind forecasts. *Mon. Wea. Rev.,* **133,** 3368–3381.

——, ——, Y. Liu, and T. T. Warner, 2004: Predictability of low-level winds by mesoscale meteorological models. *Mon. Wea. Rev.,* **132,** 2553–2569.

Schroeder, A. J., D. R. Stauffer, N. L. Seaman, A. Deng, A. M. Gibbs, G. K. Hunter, and G. S. Young, 2006: An automated high-resolution, rapidly relocatable meteorological nowcasting and prediction system. *Mon. Wea. Rev.,* **134,** 1237–1265.

Skamarock, W. C., 2004: Evaluating mesoscale NWP models using kinetic energy spectra. *Mon. Wea. Rev.,* **132,** 3019–3032.

——, J. B. Klemp, J. Dudhia, D. O. Gill, D. M. Barker, W. Wang, and J. G. Powers, 2007: A description of the advanced research WRF version 2. NCAR Tech. Note NCAR/TN-468+STR, 88 pp.

Smagorinsky, J., 1963: General circulation experiments with the primitive equations: Part I. The basic experiment. *Mon. Wea. Rev.,* **91,** 99–164.

Smedman, A.-S., 1988: Observations of a multi-level turbulence structure in a very stable atmospheric boundary layer. *Bound.-Layer Meteor.,* **44,** 231–253.

Soderberg, S., and O. Parmhed, 2006: Numerical modeling of katabatic flow over a melting outflow glacier. *Bound.-Layer Meteor.,* **120,** 509–534.

Steeneveld, G. J., B. J. H. Van de Wiel, and A. A. M. Holtslag, 2006: Modeling the evolution of the atmospheric boundary layer coupled to the land surface for three contrasting nights in CASES-99. *J. Atmos. Sci.,* **63,** 920–935.

——, ——, and ——, 2007: Diagnostic equations for the stable boundary layer height: Evaluation and dimensional analysis. *J. Appl. Meteor. Climatol.,* **46,** 212–225.

Stensrud, D. J., and S. J. Weiss, 2002: Mesoscale model ensemble forecasts of the 3 May 1999 tornado outbreak. *Wea. Forecasting,* **17,** 526–543.

Sukoriansky, S., B. Galperin, and V. Perov, 2006: A quasi-normal scale elimination model of turbulence and its application to stably stratified flows. *Nonlinear Processes Geophys.,* **13,** 9–22.

Sun, J., and Coauthors, 2002: Intermittent turbulence associated with a density current passage in the stable boundary layer. *Bound.-Layer Meteor.,* **105,** 199–219.

Sykes, R. I., S. F. Parker, D. S. Henn, and W. S. Lewellen, 1993: Numerical simulations of ANATEX tracer data using a turbulence closure model for long-range dispersion. *J. Appl. Meteor.,* **32,** 929–947.

——, ——, ——, C. P. Cerasoli, and L. P. Santos, 1998: PC-SCIPUFF version 1.2 PD technical documentation. ARAP Rep. 718, 170 pp.

Tennekes, H., and J. L. Lumley, 1972: *A First Course in Turbulence*. MIT Press, 300 pp.

Van de Wiel, J. H., A. F. Moene, O. K. Hartogensis, H. A. R. De Bruin, and A. A. M. Holtslag, 2003: Intermittent turbulence in the stable boundary layer over land. Part III: A classification for observations during CASES-99. *J. Atmos. Sci.,* **60,** 2509–2522.

Vickers, D., and L. Mahrt, 2004: Evaluating formulations of stable boundary layer height. *J. Appl. Meteor.,* **43,** 1736–1749.

Vogelezang, D. H. P., and A. A. M. Holtslag, 1996: Evaluation and model impacts of alternative boundary-layer height formulations. *Bound.-Layer Meteor.,* **81,** 245–269.

Weckwerth, T. M., and Coauthors, 2004: An overview of the International H_2O Project (IHOP_2002) and some preliminary highlights. *Bull. Amer. Meteor. Soc.,* **85,** 253–277.

Weiss, S. J., and Coauthors, 2007: The NOAA hazardous weather testbed: Collaborative testing of ensemble and convection-allowing WRF models and subsequent transfer to operations at the Storm Prediction Center. Preprints, *22nd Conf. on Weather Analysis and Forecasting/18th Conf. on Numerical Weather Prediction,* Park City, UT, Amer. Meteor. Soc., 6B.4. [Available online at http://ams.confex.com/ams/pdfpapers/124772.pdf.]

Wicker, L. J., and W. C. Skamarock, 2002: Time splitting methods for elastic models using forward time schemes. *Mon. Wea. Rev.,* **130,** 2088–2097.

Wyngaard, J. C., 2010: *Turbulence in the Atmosphere*. Cambridge University Press, 393 pp.

Young, G., B. Gaudet, N. L. Seaman, and D. R. Stauffer, 2009: Interaction of a mountain lee wave with a basin cold pool. Preprints, *13th Conf. on Mesoscale Processes,* Salt Lake City, UT, Amer. Meteor. Soc., P1.22. [Available online at http://ams.confex.com/ams/pdfpapers/155040.pdf.]

Zilitinkevich, S., I. Esau, and A. Bakalov, 2007: Further comments on the equilibrium height of neutral and stable planetary boundary layers. *Quart. J. Roy. Meteor. Soc.,* **133,** 265–271.